

# Review of Microstructure–Mechanical Property Relationships in Cast and Wrought Ni-Based Superalloys with Boron, Carbon, and Zirconium Microalloying Additions

Felix Theska,\* Wilson F. Tse, Bernd Schulz, Richard Buerstmayr, Steven R. Street, Michael Lison-Pick, and Sophie Primig\*

Cast and wrought Ni-based superalloys are materials of choice for harsh high-temperature environments of aircraft engines and gas turbines. Their compositional complexity requires sophisticated thermo-mechanical processing. A typical microstructure consists of a polycrystalline  $\gamma$ -matrix, strengthening  $\text{Ni}_3(\text{Al,Ti}) \gamma'$  precipitates, carbides (MC,  $\text{M}_6\text{C}$ , and  $\text{M}_{23}\text{C}_6$ ), borides ( $\text{M}_2\text{B}$ ,  $\text{M}_3\text{B}_2$ , and  $\text{M}_5\text{B}_3$ ), and other inclusions. Microalloying additions of B, C, and Zr commonly improve high-temperature strength and creep resistance, although excessive additions are detrimental. Grain boundary (GB) segregation may improve cohesion and displace embrittling impurities. Finely dispersed carbides and borides are desired to control grain size via GB pinning. However, excessive decoration of GBs may lead to failure during processing and in-service. Hence, a systematic review on the roles of B, C, and Zr in cast and wrought Ni-based superalloys is required. The current state of knowledge on GB segregation and precipitation is reviewed. Experimental and modeling results are compared across various processing steps. The impact of GB precipitation on mechanical properties is most well researched. Co-precipitation in proximity to GBs interacting with local microstructure evolution and mechanical properties remains less explored. Addressing these gaps in knowledge allows a more complete understanding of processing–microstructure–properties relationships in advanced cast and wrought Ni-based superalloys.

## 1. Introduction

High-performance components in aerospace and oil and gas applications must endure harsh environments at high temperatures for several thousands of hours of service.<sup>[1–3]</sup> Cast and wrought Ni-based superalloys are engineering materials designed to achieve a unique property profile of high-temperature strength, creep, and corrosion resistance. This is enabled by their compositional complexity and sophisticated manufacturing processes.<sup>[4–6]</sup> Primary and scrap materials are combined in a sequence of melting, remelting, and thermo-mechanical processing to achieve the desired composition, microstructure, and shape of components.<sup>[7–11]</sup> A typical property profile for static components in aircraft engines is a yield strength >900 MPa, elongation >30%, and creep rupture strength in 1000 h of >100 MPa at operation temperatures of  $\approx 800^\circ\text{C}$ .<sup>[12,13]</sup> Efficiency improvements for the next generation of gas turbine engines will require materials design using the highest alloyed Ni-based superalloy grades to unlock

superior high-temperature strength.<sup>[14–16]</sup> This makes cast and wrought processing more challenging due to macro-segregation, increased flow stresses, and cracking.<sup>[4–6]</sup> Furthermore, desirable increases in recycling rates for both economic and sustainability reasons create additional compositional complexity.<sup>[17–19]</sup>

A schematic of the typical microstructure of cast and wrought Ni-based superalloys is shown in **Figure 1**.  $\text{L1}_2$ -ordered, coherent  $\text{Ni}_3(\text{Al,Ti}) \gamma'$  precipitates embedded in equiaxed grains of a face-centered cubic (fcc)  $\gamma$ -matrix provide high-temperature strength via coherency strengthening.<sup>[20–22]</sup> Grain boundaries (GBs) can be decorated by  $\text{GB-}\gamma'$ ,<sup>[23–25]</sup> carbides (MC,  $\text{M}_6\text{C}$ , and  $\text{M}_{23}\text{C}_6$ ),<sup>[12,26,27]</sup> and/or borides ( $\text{M}_2\text{B}$ ,  $\text{M}_3\text{B}_2$ , and  $\text{M}_5\text{B}_3$ ).<sup>[28–30]</sup> Other inclusions present may be oxides ( $\text{Al}_2\text{O}_3$  and  $\text{ZrO}_2$ ), nitrides (TiN), sulfides (MgS, ZrS, and MoS), or carbonitrides and sulfocarbides.<sup>[31]</sup> B, C, and Zr are microalloying additions to optimize high-temperature strength and creep properties via GB segregation.<sup>[32]</sup> During vacuum induction melting (VIM), electro-

F. Theska, W. F. Tse, B. Schulz, R. Buerstmayr, S. R. Street, S. Primig  
School of Materials Science & Engineering  
UNSW Sydney  
Sydney, NSW 2052, Australia  
E-mail: f.theska@unsw.edu.au; s.primig@unsw.edu.au

W. F. Tse, S. R. Street, M. Lison-Pick  
Western Australian Specialty Alloys (WASA)  
Perth, WA 6155, Australia

 The ORCID identification number(s) for the author(s) of this article can be found under <https://doi.org/10.1002/adem.202201514>.

© 2022 The Authors. Advanced Engineering Materials published by Wiley-VCH GmbH. This is an open access article under the terms of the Creative Commons Attribution-NonCommercial License, which permits use, distribution and reproduction in any medium, provided the original work is properly cited and is not used for commercial purposes.

DOI: 10.1002/adem.202201514

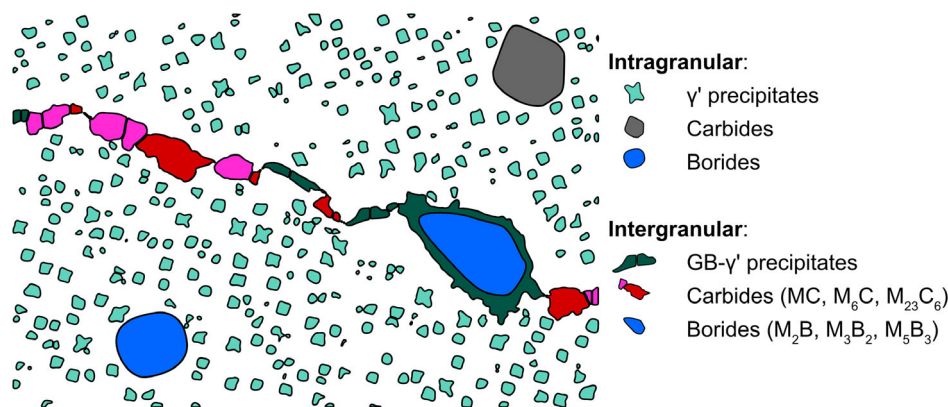


**Figure 1.** Schematic of a typical microstructure of a cast and wrought Ni-based superalloy, e.g., René 41.  $\gamma'$  precipitates are found in the grain interior and at GBs. Carbides and borides are found at GBs and in the grain interior.

slag remelting (ESR), and vacuum arc remelting (VAR), these elements are “gettering” embrittling impurities such as S, P, and O to improve ductility and strength.<sup>[33–42]</sup> In the solid state, B, C, and Zr can improve GB cohesion and displace detrimental impurities.<sup>[36–38,43,44]</sup> Excessive additions promote the formation of borides and carbides, which can be beneficial (e.g., Zener-Smith pinning & GB serrations)<sup>[39,45–49]</sup> or detrimental (e.g., GB embrittlement & GB incipient melting),<sup>[47,50–53]</sup> and thus lead to failure during manufacturing or in-service.<sup>[39,40,54–57]</sup>

GBs and their composition are important topics as  $\approx 20\%$  of publications registered by Scopus on superalloys also include GBs and B, C, or Zr. It is necessary to emphasize that the present review focuses on the roles of B, C, and Zr in cast and wrought processed Ni-based superalloys for static or rotating gas turbine engine components. Their required manufacturing processes, microstructures, and properties are considerably different from those of other superalloys, such as directionally solidified or powder metallurgically (PM) processed superalloys, which are optimized for creep and fatigue performance.<sup>[4–6]</sup> While it is valuable to explore the impact of B, C, and Zr on defect and eutectic formation in cast microstructures, they are not the focus of this review, and more details on cast and directionally solidified superalloys may be found elsewhere.<sup>[34,58]</sup> However, defect structures altered by microalloying may be passed on to subsequent processing and thus potentially impact the effectiveness of homogenization, hot working, and heat treatment. For example, carbide clusters and porosity may promote forge cracking and void nucleation.<sup>[31,41,47,59]</sup> This highlights the complexity of the detailed roles of B, C, and Zr in cast and wrought Ni-based superalloys. A comprehensive review on their microalloying is currently missing. Several other reviews on Ni-based superalloys are available. Challenges in the processing of cast and wrought Ni-based superalloys are comprehensively presented by Hardy et al.<sup>[13]</sup> However, the impact of B, C, and Zr was not discussed. Yang et al.<sup>[31]</sup> reviewed inclusions in cast and wrought Ni-based superalloys but acknowledged that more research is required to gain a more complete understanding of their thermodynamic and kinetic properties. Welding and additive manufacturing (AM) of Ni-based superalloys have been reviewed extensively,<sup>[60–62]</sup> but process conditions and phase transformation kinetics vary considerably from cast and wrought

processing. The impact of B, C, and Zr on the creep resistance of Ni-based superalloys is studied most frequently.<sup>[54,63–65]</sup> While some of these insights are transferrable, significant differences in thermo-mechanical history to cast and wrought processing must be acknowledged. First-principles and thermodynamic modeling have helped to rationalize the roles of microalloying elements at GBs.<sup>[7,26,36–38,43,66,67]</sup> However, computational constraints and necessary model simplifications may limit their explicit applicability to industrial processing. Direct experimental observations of GB segregation remain challenging, but recent advances in characterization and data analysis methods enable a more detailed understanding of the roles of microalloying elements.<sup>[68–71]</sup> Nanoscale secondary ion mass spectrometry (Nano-SIMS), electron energy loss spectroscopy (EELS), or atom probe microscopy (APM) allow quantitative characterization, including light elements, such as B and C.<sup>[72]</sup> Energy-dispersive X-Ray spectroscopy (EDXS) or electron probe micro-analysis (EPMA) can be applied to characterize heavy elements.<sup>[73,74]</sup>

This review attempts to summarize current knowledge on the roles of the microalloying elements B, C, and Zr. A systematic approach is required to understand these elements within the complex processing–microstructure–property relationships of cast and wrought Ni-based superalloys. We first introduce each microalloying element individually with its electronic structure and roles during cast and remelting processes. In the solid state, GB segregation and GB precipitation are reviewed, both covered by experimental findings and modeling work. Then, the combined impact of B, C, and Zr is reviewed with regard to solid-state micro-segregation, phase transformations, processability, and properties. Finally, important areas for future research with respect to cast and wrought processing of Ni-based superalloys are presented before concluding remarks are made.

## 2. Boron

### 2.1. Segregation

B exhibits a relatively small covalent radius of 0.082 nm (for comparison, the covalent radius of Ni is 0.121 nm).<sup>[75]</sup>  $^{10}\text{B}$  and  $^{11}\text{B}$  are the only naturally stable isotopes, and most chemical and metallurgical properties are dictated by the electron

configuration of its three valence electrons ( $2s^2 2sp^1$ ) in  $sp^2$  hybridization. B additions have been shown to achieve desirable properties in Ni-based superalloys and therefore may be added intentionally. During melting and casting, B additions may improve the fluidity.<sup>[9]</sup> However, solidification cracking may occur due to incipient melting point depression, as shown by differential thermal analysis (DTA) or differential scanning calorimetry (DSC).<sup>[10]</sup> Limited solute exchange between liquid and solid phases promotes eutectic solidification microstructures and deteriorates the creep resistance.<sup>[10,11,76]</sup> In the solid state, low solid solubility of B in Ni and its affinity to segregate to GBs are well documented.<sup>[48,77–81]</sup> Such micro-segregation is driven by changes in the reduction of interfacial free energy (equilibrium segregation) or vacancy annihilation from atom–vacancy complexes (nonequilibrium segregation).<sup>[32]</sup> Improvements to hot workability and creep resistance were reported by Decker et al.<sup>[82]</sup> Decker & Freeman<sup>[83]</sup> also proposed that B and Zr prevent the agglomeration of  $M_{23}C_6$  carbides and  $\gamma'$  precipitates at GBs. As result, linking of micro-cracks into networks is hindered and creep resistance is improved. Cottrell<sup>[84]</sup> considered small amounts of B beneficial in suppressing GB embrittlement in Ni, Fe, and  $Ni_3Al$ . This was attributed to the electronic properties of B. Floreen & Davidson<sup>[85]</sup> suggested that the primary effect of B is the displacement of GB embrittling elements, such as O, and thus, reducing the interfacial energy. This can suppress micro-cracking at GBs.

Direct experimental verification of B micro-segregation remains challenging. For example, SIMS or nano-SIMS maps are suitable for comparative studies.<sup>[8,63,79]</sup> Figure 2a shows an example of SIMS mapping to reveal the impact of GB serrations limiting B segregation in Alloy 263.<sup>[79]</sup> As result, serrated GBs were found less susceptible to GB liquation cracking during welding. Quantitative, three-dimensional mapping can be obtained from APM as demonstrated in Figure 2b.<sup>[80,86,87]</sup> This example showcases the direct local compositional measurement across a  $\gamma$ -matrix/ $\gamma'$  precipitate phase boundary in proximity to a GB in Astroloy. Advanced APM analysis techniques have been developed that allow the direct quantification of the interfacial excess.<sup>[88,89]</sup> Other relevant analytical methods are field ion microscopy (FIM), which is closely related to APM, or Auger electron spectroscopy (AES) on free surfaces. However, the quantification of interfacial excess across boundaries of phases with different solute solubilities, e.g., B at the  $\gamma$ -matrix/carbide interface remain to be explored.

First-principles calculations have been the most successful technique for assessing the impact of GB segregation on the mechanical properties. The interaction of dislocations with GBs as well as GB sliding, e.g., during creep, can be assessed using molecular dynamics.<sup>[90–94]</sup> Cleavage energy and (partial) cohesive energy are calculated to gauge the resistance against GB decohesion.<sup>[36–38,43]</sup> Table 1 provides a brief summary of first-principles calculations on B in Ni.<sup>[36,43,95]</sup> For example, GB segregation energies of around  $-1.2$  eV atom<sup>-1</sup> correlate well with the experimentally observed affinity of B toward GB segregation.<sup>[38,43,44,95,96]</sup> Sanyal et al.<sup>[36]</sup> calculated changes in GB segregation and cleavage energies of a  $\Sigma 5(012)$  boundary in Ni for B, C, S, Cr, and Hf. S was shown to be the most detrimental, and B the most promising element by changing the cleavage energy by  $-11$  and  $+6\%$ , respectively. Razumovskiy et al.<sup>[43]</sup>

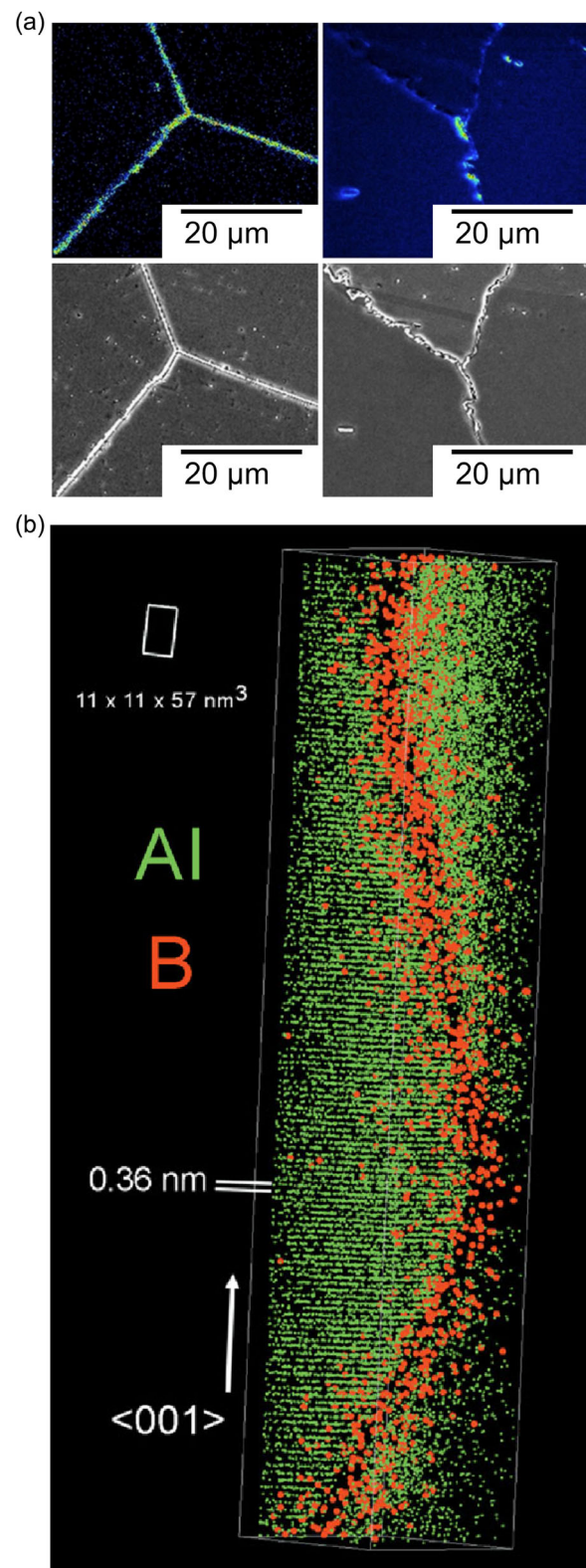


**Figure 2.** a) SIMS maps of B in a hot rolled Alloy 263 with serrated and GBs. Adapted with permission.<sup>[79]</sup> Copyright 2011, Springer Nature. b) APM reveals GB segregation of B with near-atomic resolution in Astroloy. Adapted with permission.<sup>[80]</sup> Copyright 2007, Cambridge University Press.

**Table 1.** Overview of B impacting the GB segregation, GB strengthening, and partial cohesive energies.

GB segregation energy [eV atom <sup>-1</sup> ]	GB strengthening energy [eV atom <sup>-1</sup> ]	Partial cohesive energy [eV atom <sup>-1</sup> ]	References
–	–0.4	–	[36,38]
–1.7	–0.7	(–) 0.8 to –1.6	[38,43,44]
0 to –2.3	–1.0	–	[95]
–0.4 to –1.8	–	–	[96]

calculated the segregation and partial cohesive energies for the same type of GB. B, Zr, and Hf were found to increase the bond strength, while S and Bi were found to be the most detrimental. Some constraints of these models include calculations at temperatures of 0 K, observation of few unit cells,<sup>[36]</sup> few 100s of atoms,<sup>[37]</sup> or the use of periodic supercells reaching ≈20 atomic layers.<sup>[38,43]</sup> However, satisfying agreement between experimental studies and first-principles calculations is reported.<sup>[95,96]</sup>

## 2.2. Boride Precipitation

B additions exceeding ≈0.01 wt% may promote the formation of borides.<sup>[39,63,97]</sup> Borides are formed with metal formers M such as Mo, Ti, Cr, Co, and Ni. In Ni-based superalloys, M<sub>2</sub>B, M<sub>3</sub>B<sub>2</sub>, and M<sub>5</sub>B<sub>3</sub> are commonly observed.<sup>[28–30,39,65,98]</sup> Their structural and compositional information are summarized in **Table 2**. Exemplary unit cells and their typical blocky morphologies observed in scanning electron microscopy (SEM) and transmission electron microscopy (TEM) micrographs are provided in **Figure 3**.<sup>[30,40,64,99–101]</sup> M<sub>2</sub>B is the least frequently reported boride in Ni-based superalloys and may be Cr- or Mo-rich, depending on the superalloy composition.<sup>[40,65,81,98]</sup> M<sub>2</sub>B exhibits polytypes of a C16 body-centered tetragonal crystal structure (see **Figure 3a**) and a C<sub>b</sub> face-centered orthorhombic crystal structure.<sup>[28,98]</sup> Mo-rich M<sub>2</sub>B as shown in **Figure 3b** has been reported in polycrystalline Ni-based superalloys using FIM and APM.<sup>[40,81]</sup> Intergrowth of variants and high concentrations of stacking faults have been observed in M<sub>2</sub>B experiencing rapid thermal gradients during AM or welding.<sup>[28,65]</sup> During long-term exposure, M<sub>2</sub>B borides are considered to be stable against decomposition by first-principles calculations, thermo-kinetic modeling, and experimental observations.<sup>[40,81,102]</sup>

M<sub>3</sub>B<sub>2</sub> and M<sub>5</sub>B<sub>3</sub> borides are more commonly reported in Ni-based superalloys.<sup>[29,30,39,50,103–105]</sup> Mo-rich M<sub>3</sub>B<sub>2</sub> borides have a D5<sub>a</sub> tetragonal crystal structure (see **Figure 3c**) that can be constituted by the general L<sub>2</sub>SB<sub>2</sub> structure where L represents elements with larger atomic radii such as W, Mo, and Ti, while S represents elements with smaller atomic radii such as Cr, Co,

and Ni.<sup>[30,103,106]</sup> Their blocky morphology is shown in **Figure 3d**.<sup>[30]</sup> In cast IN939 and Udimet 700, M<sub>3</sub>B<sub>2</sub> borides have been linked to the formation of eutectic pools once the incipient melting temperature is exceeded.<sup>[50,51]</sup> Similarly, constitutional liquation during high heating rates is reported in welding literature.<sup>[107]</sup> This can be detrimental to the hot workability and demonstrates the necessity for proper homogenization treatments between (re-)melting and wrought processing.

Cr-rich M<sub>5</sub>B<sub>3</sub> borides have a D8<sub>1</sub> tetragonal crystal structure (see **Figure 3e**) and may be represented as the general L<sub>4</sub>SB<sub>3</sub> structure.<sup>[30,63]</sup> GB precipitation of M<sub>5</sub>B<sub>3</sub> in polycrystalline Ni-based superalloys has been shown to improve their ductility.<sup>[39,63]</sup> Micromechanical testing revealed that this is due to interlocked GB serrations, as shown in **Figure 3f**. However, M<sub>5</sub>B<sub>3</sub> has been observed to decompose or coarsen during long-term high-temperature exposure.<sup>[54,108]</sup> Du et al.<sup>[108]</sup> reported in Equation (1), a decomposition reaction whereby M<sub>5</sub>B<sub>3</sub> captures Cr and C and releases Mo and B in order to form M<sub>23</sub>C<sub>6</sub> carbides



First-principles calculations by Sanyal et al.<sup>[37]</sup> also showed that the susceptibility to oxygen-induced GB embrittlement was lower at Cr<sub>5</sub>B<sub>3</sub>/Ni interfaces.<sup>[37]</sup> Xia et al.<sup>[102]</sup> calculated the shear moduli, Young's moduli, and hardness for the above-mentioned borides. Generally, a trend of M<sub>3</sub>B<sub>2</sub> > M<sub>5</sub>B<sub>3</sub> > M<sub>2</sub>B is followed for elements substituting M as Cr > W > Mo. For example, Cr<sub>3</sub>B<sub>2</sub> and Cr<sub>5</sub>B<sub>3</sub> would exhibit the highest hardness, while Mo<sub>2</sub>B and W<sub>2</sub>B would exhibit the lowest hardness.

## 3. Carbon

### 3.1. Segregation

The covalent radius of C with 0.077 nm is considerably smaller than that of B.<sup>[109,110]</sup> <sup>12</sup>C and <sup>13</sup>C are the only stable isotopes. Its chemical and metallurgical properties are dictated by its electron configuration of four valence electrons (2s<sup>2</sup> 2p<sup>2</sup>), which allow for different hybridizations: sp in poly-ine, sp<sup>2</sup> in hexagonal, and sp<sup>3</sup> in cubic coordination. Low solid solubility and the tendency to segregate toward GBs in Ni-based superalloys are frequently reported.<sup>[40,49,57,64,111–113]</sup>

C is a multipurpose minor alloying element commonly added to cast and wrought Ni-based superalloys in a typical range of 0.02–0.18 wt% to reduce processing defects and enhance high-temperature mechanical properties such as creep resistance and stress rupture to failure.<sup>[34]</sup> During melting and casting processing, such as VIM, C additions improve the purity by removing tramp elements such as O and S.<sup>[34,114]</sup> Similar to B additions, improvements to fluidity during casting have been reported.<sup>[115]</sup>

**Table 2.** Overview of three commonly observed borides in polycrystalline Ni-based superalloys.

Phase	Space group	Crystallographic parameters	Structure	References
M <sub>2</sub> B	I 4/m c m (140)	a = 0.557 nm, c = 0.474 nm	C16 (Mo,Cr) <sub>2</sub> B	[28,81,98]
	F d d d (70)	a = 1.471 nm, b = 0.741 nm, c = 0.425 nm	C <sub>b</sub> Cr <sub>2</sub> B	
M <sub>3</sub> B <sub>2</sub>	P 4/m b m (127)	a = 0.576 nm, c = 0.304 nm	D5 <sub>a</sub> (Mo,Cr) <sub>3</sub> B <sub>2</sub>	[29,30,48]
M <sub>5</sub> B <sub>3</sub>	I 4/m c m (140)	a = 0.546 nm, c = 1.064 nm	D8 <sub>1</sub> Cr <sub>5</sub> B <sub>3</sub>	[29,30,54]

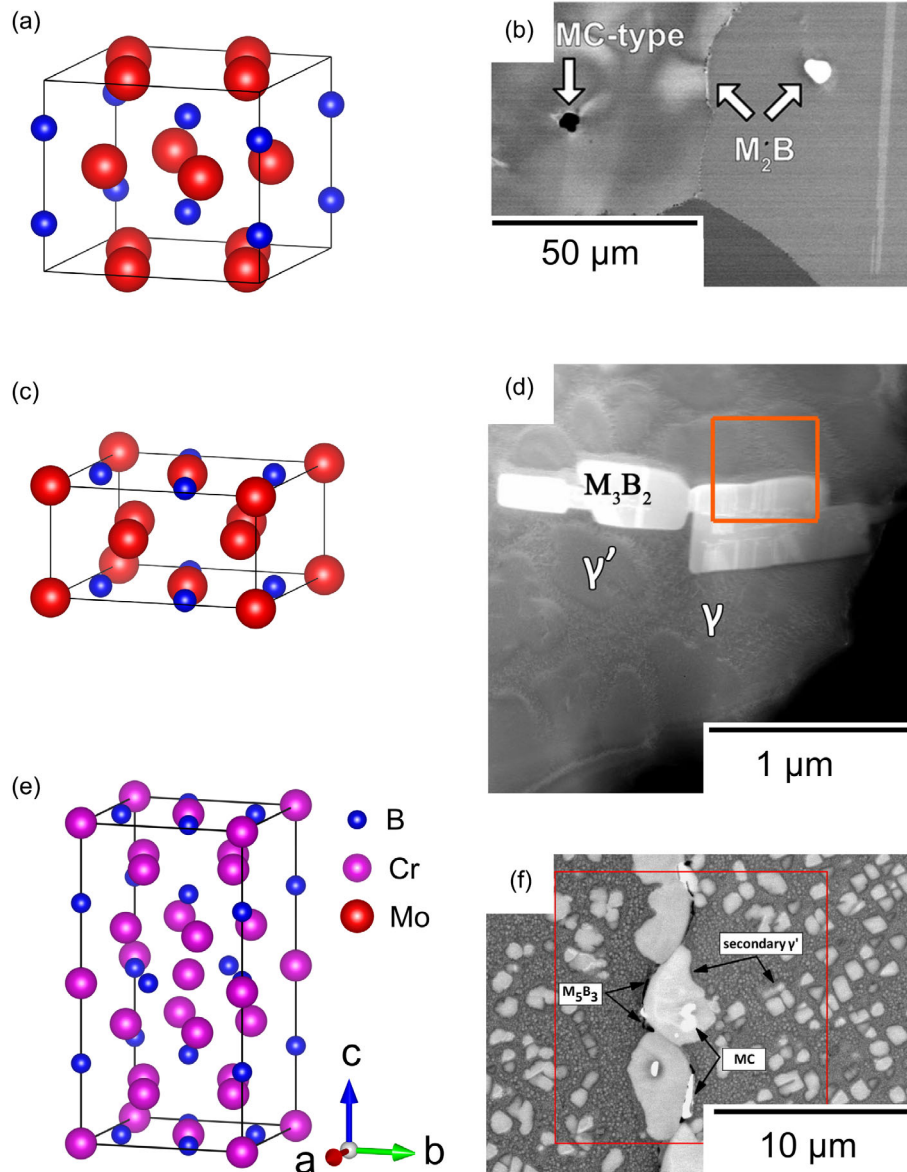


**Figure 3.** a) Unit cell of C16-ordered  $M_2B$  boride,<sup>[99]</sup> b)  $M_2B$  borides observed at GBs and grain interiors in a René 41 superalloy. Adapted with permission.<sup>[40]</sup> Copyright 2022, Elsevier. c) Unit cell of Mo-rich  $M_3B_2$  boride,<sup>[100]</sup> d) TEM micrograph of blocky  $M_3B_2$  borides. Adapted under the terms of the CC BY 4.0 license.<sup>[30]</sup> Copyright 2014, Springer Nature. e) Unit cell of Cr-rich  $M_5B_3$  boride,<sup>[101]</sup> f)  $M_5B_3$  borides decorating GBs in a B-containing STAL15-CC prototype superalloy. Adapted under the terms of the CC BY 4.0 license.<sup>[39]</sup> Copyright 2017, Elsevier.

C may promote the  $\gamma + \gamma'$  eutectic,<sup>[115,116]</sup> which can result in hot tearing and stress relief cracking,<sup>[111]</sup> or shrinkage porosity.<sup>[117]</sup> Cottrell<sup>[84]</sup> found C segregation to have an embrittling effect in  $Ni_3Al$  and first assumed excessive GB segregation of C may result in the formation of graphite-like structures; however, experimental verification remains lacking. Instead, TEM EELS analyses, as shown in **Figure 4a,d**, show that GB segregation of C can depend on the character and morphology of GBs.<sup>[49]</sup> This example demonstrates discontinuous C segregation at serrated GBs before the onset of carbide precipitation, correlating with an increased cracking resistance. APM studies of GBs showed that C segregation is consistently lower than B segregation.<sup>[40,57,64,111,112]</sup> The example in Figure 4e–g provides

an atom probe reconstruction of a GB in an AM Ni-based superalloy.<sup>[111]</sup> Here, B segregation reaches up to 7 at%, while C segregation reaches only about 1 at%. GB segregation of C and other impurities is also believed to act as nucleation sites for fan-shaped GB- $\gamma'$  impacting the hot deformation behavior of cast and wrought Ni-based superalloys.<sup>[118–122]</sup> However, the detailed nucleation mechanism has not been experimentally verified yet.

First-principles calculations studying GB segregation of C in Ni or Ni-based superalloys are less frequently found when compared to B. **Table 3** provides a brief overview.<sup>[36,95,96]</sup> GB segregation energies calculated by Yamaguchi et al.<sup>[95]</sup> and Ebner et al.<sup>[96]</sup> are lower than those of B and correlate well with

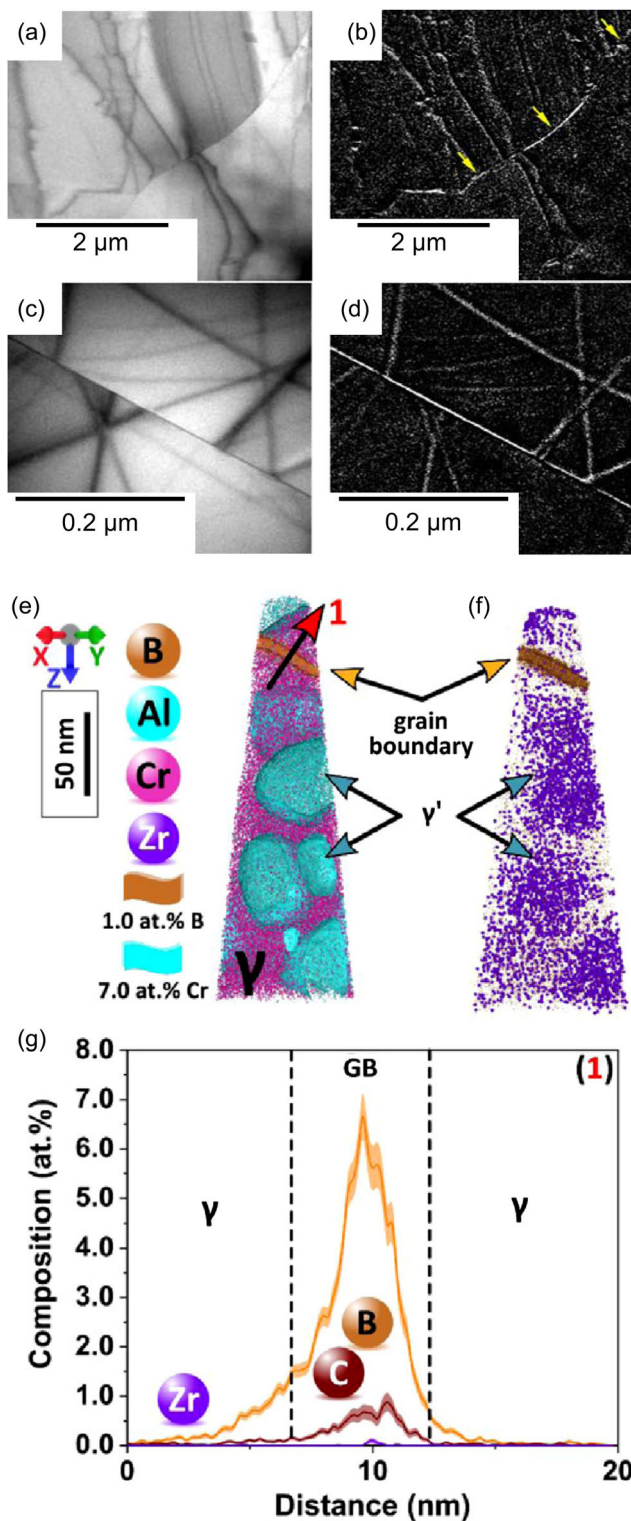


**Figure 4.** a,b) TEM micrograph and EELS map of discontinuous C segregation before  $M_{23}C_6$  precipitation at a serrated GB, c,d) TEM micrograph and EELS map at a GB without serrations in Alloy 263. Adapted with permission.<sup>[49]</sup> Copyright 2012, John Wiley and Sons. e,f) APM reconstruction of a GB in a polycrystalline AM Ni-based superalloy, g) 1D concentration profile shows C and B segregation. Adapted under the terms of the CC BY 4.0 license.<sup>[111]</sup> Copyright 2021, Elsevier.

**Table 3.** Overview of C impacting the GB segregation, GB strengthening, and partial cohesive energies.

GB segregation energy [eV atom <sup>-1</sup> ]	GB strengthening energy [eV atom <sup>-1</sup> ]	Partial cohesive energy [eV atom <sup>-1</sup> ]	References
0 to -0.8	-0.2	-	[95]
-0.1 to -0.8	-	-	[96]

experimental APM observations. Sanyal et al.<sup>[36]</sup> calculated a small and detrimental change in GB cleavage energy. The GB strengthening energy (provided in ref. [95] as embrittling potency energy) is also considerably lower than that of B. Therefore, the significance of C in cast and wrought Ni-based superalloys may be attributed to the precipitation of carbides instead of GB segregation. Some model constraints are mentioned in Section 2.1 and satisfying agreement between experimental studies and first-principles calculations is reported.<sup>[95,96]</sup>

### 3.2. Carbide Precipitation

Besides borides, carbides are one of the most common intermetallic compounds that can be found at GBs of cast and wrought Ni-based superalloys. Three different carbides are commonly observed: 1) Primary MC carbides, 2) secondary  $M_6C$  carbides, and 3) secondary  $M_{23}C_6$  carbides.<sup>[4-6]</sup>

Primary MC carbides are predominantly formed during the solidification process. They commonly consist of B1-ordered TiC with a NaCl crystal structure as illustrated in Figure 5a,b. M can also represent Ta, Hf, Zr, Nb, V, Cr, Mo, and W.<sup>[123]</sup> Most of the MC carbides share the same crystal structure as TiC except for MoC and WC that exhibit a hexagonal crystal structure. The formation from refractory metals, such as Ti, Mo, and W, imparts their high thermal stability, while the NaCl or hexagonal crystal structure is embrittling. During hot deformation, various phenomena around MC carbides including fragmentation,<sup>[27,124,125]</sup> nucleation of recrystallized grains,<sup>[126,127]</sup> and Zener–Smith pinning<sup>[45,46]</sup> have been observed.  $M_6C$  and  $M_{23}C_6$  are secondary carbides formed primarily via solid-state phase transformations during thermo-mechanical processing.<sup>[128-130]</sup> Mo-rich  $M_6C$  carbides have a E9<sub>3</sub> ordered  $A_3B_3C$  crystal structure and tend to form blocky, discrete particles between 815 and 1100 °C,<sup>[6,127,128]</sup> as shown in Figure 5c,d. They have been observed to form in Ni-based superalloys with a combined (Mo + W) content of over 6 wt%.<sup>[128]</sup> Depending on the superalloy composition, Ni, Co, Cr, Fe, Mn, Al, and V tend to substitute for A and Mo or W substitute for B. However, Nb, Ti, Ta, and Zr may also be observed.  $M_6C$  also have been described as  $\eta$  carbides and can adopt stoichiometries, such as  $A_2B_4C$  and  $A_4B_2C$ .<sup>[128,131,133,134]</sup> Thermodynamic models may assume four sublattices for improved description of substitutional and interstitial species.<sup>[135]</sup>  $M_6C$  is usually not considered detrimental to processability and can provide beneficial GB pinning.<sup>[136]</sup> More recently, Jiang et al.<sup>[137]</sup> discovered nano-twinning in  $M_6C$  as potential strengthening mechanism within such carbides. Cr-rich  $M_{23}C_6$  carbides are more commonly observed. Their crystal structure is D8<sub>4</sub> ordered  $Cr_{23}C_6$ , as shown in Figure 5e. A TEM micrograph and corresponding selected area electron diffraction (SAED) pattern

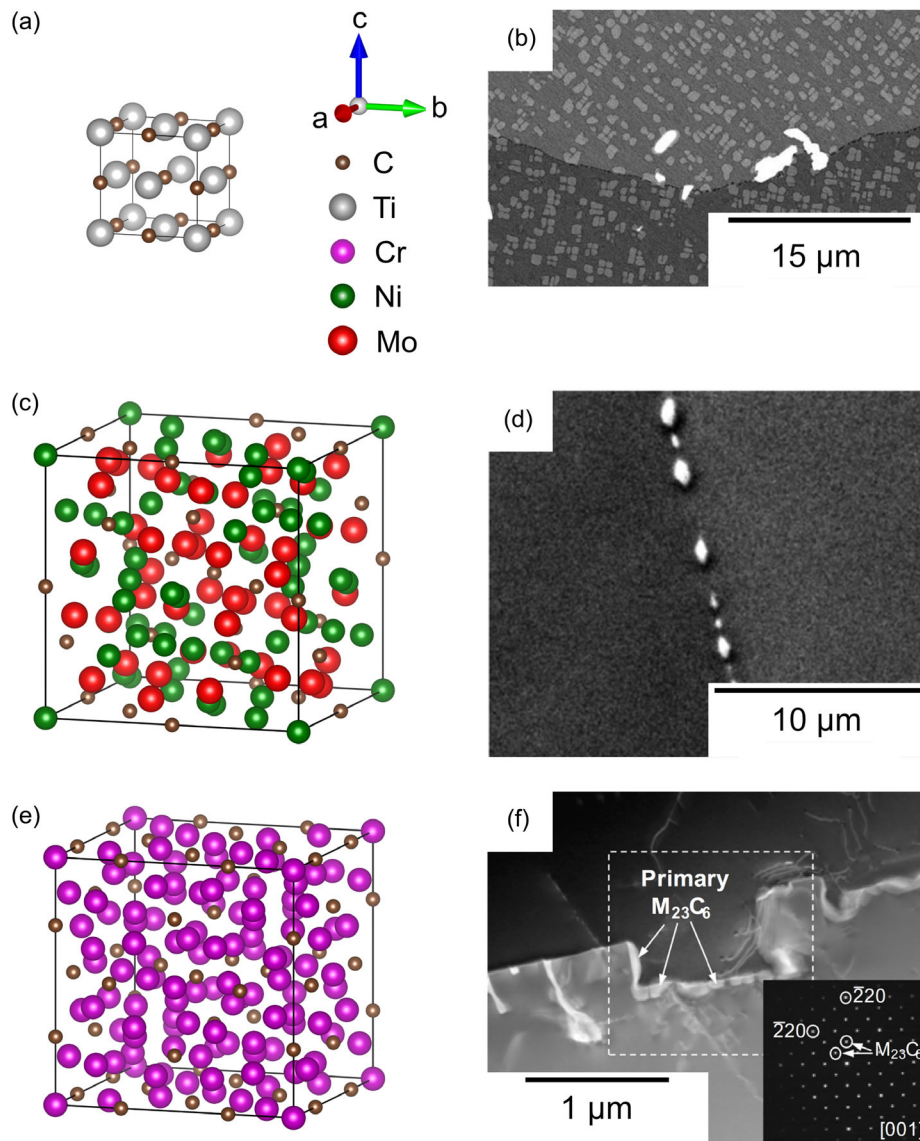


**Figure 5.** a) Unit cell of B1-ordered MC carbide,<sup>[140]</sup> b) SEM micrograph of MC carbides at GBs of a polycrystalline Ni-based superalloy. Adapted under the terms of the CC BY 4.0 license.<sup>[63]</sup> Copyright 2016, Elsevier. c) Unit cell of E9<sub>3</sub> ordered M<sub>6</sub>C carbide,<sup>[141]</sup> d) SEM micrograph of blocky, discrete M<sub>6</sub>C carbides decorating a GB. Adapted with permission.<sup>[26]</sup> Copyright 2021, Elsevier. e) Unit cell of D8<sub>4</sub> ordered M<sub>23</sub>C<sub>6</sub> carbide,<sup>[142]</sup> f) TEM micrograph of near-continuous, film-like M<sub>23</sub>C<sub>6</sub> decorating a GB; SAED pattern is shown as inset. Adapted with permission.<sup>[52]</sup> Copyright 2012, Elsevier.

provide the typically observed morphology and crystal structure in Figure 5f. While Cr usually substitutes for M in M<sub>23</sub>C<sub>6</sub>, other elements such as Al, Ti, Co, Ni, Mo, Ta, and W may be found, depending on the superalloy composition.<sup>[128,138,139]</sup> They are formed in lower temperature ranges between 760 and 1090 °C.<sup>[6,132]</sup> It has also been observed that significant amounts of C can be substituted by B, resulting in a M<sub>23</sub>(C,B)<sub>6</sub> stoichiometry.<sup>[26,54]</sup>

Unlike M<sub>6</sub>C, M<sub>23</sub>C<sub>6</sub> tends to form near-continuous GB films that can be detrimental to mechanical properties due to GB embrittlement.<sup>[47,52,53]</sup> The M<sub>23</sub>C<sub>6</sub> precipitation kinetics are also considerably faster compared to M<sub>6</sub>C.<sup>[143]</sup> During hot deformation, Zener–Smith pinning<sup>[47]</sup> and merging of M<sub>23</sub>C<sub>6</sub> carbides have been observed.<sup>[144]</sup> Cr-rich, D10<sub>1</sub> ordered M<sub>7</sub>C<sub>3</sub> carbides

are uncommon in cast and wrought Ni-based superalloys but are observed during welding and casting of Co-based superalloys.<sup>[145–148]</sup> An overview of the crystal structures of MC, M<sub>6</sub>C, and M<sub>23</sub>C<sub>6</sub> carbides is provided in Table 4.

**Table 4.** Overview of the three commonly observed carbides in polycrystalline Ni-based superalloys.

Phase	Space group	Crystallographic parameters	Structure	References
MC	F m -3 m (225)	$a = 0.432 \text{ nm}$	B1 (Ti,Zr)C	[63,140]
M <sub>6</sub> C	F d -3 m (227)	$a = 1.114 \text{ nm}$	E9 <sub>3</sub> Ni <sub>3</sub> Mo <sub>3</sub> C	[26,141]
M <sub>23</sub> C <sub>6</sub>	F m -3 m (225)	$a = 1.064 \text{ nm}$	D8 <sub>4</sub> (Cr,Mo) <sub>23</sub> (C,B) <sub>6</sub>	[52,142]

Most  $M_6C$  and  $M_{23}C_6$  carbides are believed to form from C segregation at GBs. However, MC carbides also have been observed as an important “C reservoir” promoting the formation of secondary carbides via the decomposition reactions (2) and (3).<sup>[128,149–151]</sup> While this provides C required to form  $M_6C$  or  $M_{23}C_6$ , the released Ti may also promote the formation of  $\gamma'$  precipitates. More complex carbide decomposition reactions are involved in the formation of topologically close packed (TCP) phases during long-term high-temperature exposure that is not considered here.



## 4. Zirconium

### 4.1. Segregation

Zr exhibits a covalent radius of 0.160 nm, which is considerably larger than the radii of B, C, and Ni.<sup>[109]</sup>  $^{90}\text{Zr}$ ,  $^{91}\text{Zr}$ ,  $^{92}\text{Zr}$ , and  $^{94}\text{Zr}$  are stable isotopes. Chemical as well as metallurgical properties are dictated by the electron configuration of its four valence electrons ( $4d^2 5s^2$ ). However, the relatively low number of d electrons may not provide strong bonds, and the low electronegativity of 1.4 favors oxidation to  $\text{Zr}^{+4}$  instead. Due to its metallic properties, the role of Zr in cast and wrought Ni-based superalloys is assumed to be different from B and C and remains somewhat controversial. Generally, GB segregation and solubility of Zr in various precipitates have been reported.<sup>[40,64,76,111,152,153]</sup>

During VIM, one important mechanism is “gettering” of S and O to mitigate their harmful effects.<sup>[34,154]</sup> In combination with C, this may result in the formation of sulfo-carbides,<sup>[34]</sup> although these phases may not be retained at GBs in cast and wrought Ni-based superalloys. Similar to B and C, Zr additions may promote the formation of a  $\gamma + \gamma'$  eutectic during the casting process.<sup>[11,155,156]</sup> This may result in weak intergranular coalescence and promote hot tearing. In the solid state, Zr is commonly associated with B as GB strengtheners. GB segregation of Zr is frequently observed in Ni-based superalloys with Zr additions.<sup>[40,64,111,112]</sup> In such alloys, it may dissolve into carbides, as shown by an SEM micrograph and EDXS map in **Figure 6a,b**.<sup>[152]</sup> The resulting carbide refinement can be beneficial in mitigating the brittleness of carbides. White et al.<sup>[154]</sup> reported improvements in creep ductility due to Zr forming precipitates assumed to be ZrS. Besides carbides, Zr may also dissolve in  $\gamma'$  precipitates. More details on co-precipitation will be discussed in the next section. A comparison between B, C, and Zr GB segregation is presented **Figure 6c–e**.<sup>[112]</sup> Using transmission Kikuchi diffraction (TKD), high-angle GBs (HAGBs) can be identified during focused ion beam (FIB) site-specific sample preparation.<sup>[157,158]</sup> Hariharan et al.<sup>[112]</sup> used this approach to quantify the interfacial excess at HAGBs for standard IN738LC and Si-modified IN738LC. This showed that Zr appears less sensitive to the GB misorientation, when compared to B, C, or Si. Some of the current authors found that Zr GB segregation weakly correlates with the Zr content in a René 41 superalloy, indicating that it is instead dissolved in  $\gamma'$  precipitates.<sup>[40]</sup>

Després et al.<sup>[64,111]</sup> showed a similar behavior in AD730 during AM. Zr additions may improve GB cohesion, decrease diffusion, and reduce carbide agglomeration.<sup>[152]</sup>

The impact of Zr on GB cohesion has been researched using first-principles calculations.<sup>[38,95,96,159]</sup> **Table 5** provides a summary of reported energies. Razumovskiy et al.<sup>[38]</sup> and Yamaguchi et al.<sup>[95]</sup> found similar cohesive energies in Ni. Xue et al.<sup>[160]</sup> found that Zr significantly reduces the GB energy. Interestingly, they also reported the potential of Zr to cosegregate with Ta, Re, or Cu toward  $\Sigma 5[001]$  GBs.<sup>[159]</sup> The GB segregation energy for Zr is similar to B and considerably lower than that of C. However, its GB strengthening energy is similarly low as that reported for C. The partial cohesive energy is lower than reported for B. Thus, Zr tends to exhibit a strong affinity toward GBs, similar to B, but its strengthening or cohesive benefit may be lower than that of B. Instead of directly affecting GBs via micro-segregation, the role of Zr is dominated by its dissolution in, promotion, or suppression of GB precipitates, as outlined in the following section. More recent studies could calculate larger volumes reaching 15 unit cells.<sup>[159,160]</sup> Overall, satisfying agreement with experimental studies is reported.<sup>[38,159]</sup>

### 4.2. Precipitation of Zr-Rich Phases

Sulfides and sulfo-carbides may result from Zr reacting with tramp elements, but Zr additions may also promote the precipitation of other phases. A commonly observed Zr-rich phase is ZrC as shown in **Figure 7a,b**. It has an NaCl crystal structure similar to that of MC carbides, but is thermodynamically more stable.<sup>[148]</sup> Hence, Zr can stabilize MC carbides and prevent decomposition into detrimental TCP phases during long-term high-temperature exposure.<sup>[54]</sup> Zr also impacts the growth and morphology of GB precipitates. Tsai et al.<sup>[152]</sup> reported carbide refinement by Zr additions. This correlates well with Zhou et al.<sup>[161]</sup> reporting a change of MC carbide morphology from script like to blocky due to Zr additions. In a variant of IN718, Zr additions may promote a blocky Laves phase morphology.<sup>[9]</sup> The affinity of Zr toward O can result in the formation of  $\text{ZrO}_2$ . **Figure 7c,d** provides an examples of monoclinic  $m\text{-ZrO}_2$  occasionally found in polycrystalline Ni-based superalloys.<sup>[31,111,162–166]</sup> A number of studies on PM processed Ni-based superalloys report on  $\text{ZrO}_2$ .<sup>[164–166]</sup> Here, its role as nucleation site for MC carbides may depend on individual superalloy composition and thermo-mechanical processing. Després et al.<sup>[111]</sup> showed that Zr partitions into  $m\text{-ZrO}_2$  as result of a reaction reducing  $\text{Al}_2\text{O}_3$  inclusions during AM. Zr can also promote the formation of  $\gamma'$  precipitates.<sup>[40,64,153,167]</sup> This is shown exemplary in **Figure 7e,f**, where Zr may replace the Ni sites  $\gamma'$  precipitates, yielding a stoichiometry of  $(\text{Ni,Zr})_3(\text{Al,Ti})$ .

A brief overview of precipitates commonly promoted by Zr is provided in **Table 6**. Their crystallographic parameters may depend on the exact superalloy composition and precipitate stoichiometry. For example, this is a well-known impact on the lattice mismatch of  $\gamma'$  precipitates to the  $\gamma$ -matrix.<sup>[40,111,153,171]</sup> In comparison to TiC, the lattice parameter of ZrC is noticeably larger,<sup>[111,140,168]</sup> and variations in the lattice parameters of  $m\text{-ZrO}_2$  follow a similar trend.<sup>[111,170]</sup>

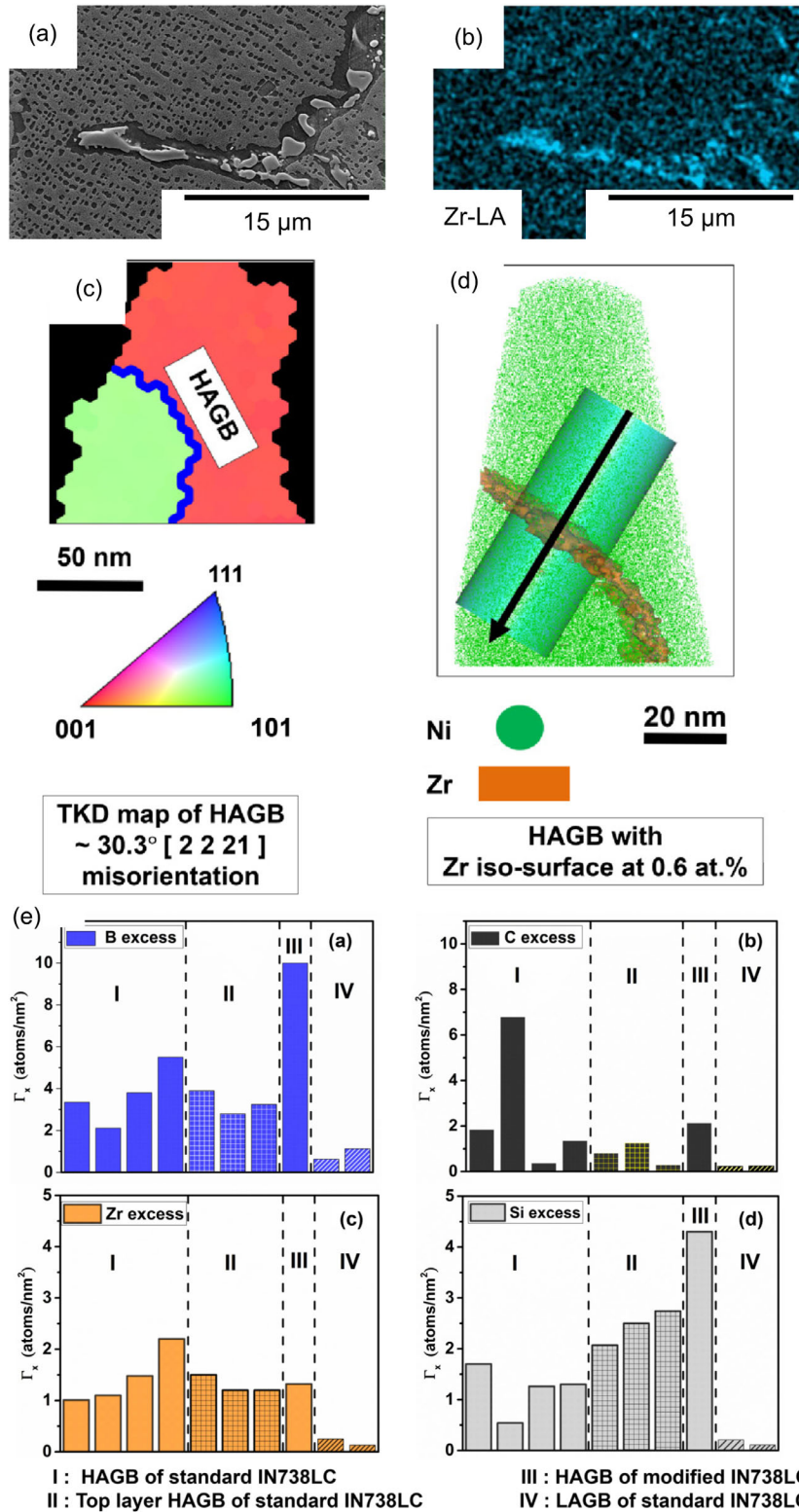


**Figure 6.** a) SEM micrograph of carbides in a fine-grained Ni-based superalloy, b) EDXS mapping reveals Zr segregation in carbides if Zr content. Adapted with permission.<sup>[152]</sup> Copyright 2014, Elsevier. c) TKD map of an APM specimen shows a HAGB with  $30.3^\circ$  misorientation, d) APM reconstruction with Ni atoms in green and a 0.6 at.% Zr iso-concentration surface, e) Interfacial excess from APM reconstructions reveal Zr GB segregation is less sensitive than B or C. Adapted under the terms of the CC BY 4.0 license.<sup>[112]</sup> Copyright 2019, American Physical Society.

**Table 5.** Overview of Zr impacting the GB segregation, GB strengthening, and partial cohesive energies.

GB segregation energy [eV atom <sup>-1</sup> ]	GB strengthening energy [eV atom <sup>-1</sup> ]	Partial cohesive energy [eV atom <sup>-1</sup> ]	References
-2.1	-0.1	-2.1	[38]
0.2 to -1.0	-	(-) 3.3	[43]
-1.3 to -2.2	-	-	[159]

## 5. Combined Impacts of Boron, Carbon, and Zirconium

### 5.1. Solid-State Microsegregation

The selection of common commercial cast and wrought Ni-based superalloys in **Table 7** highlights their compositional complexity. However, this selection cannot be regarded exhaustive as ongoing superalloy design, and development efforts produce many

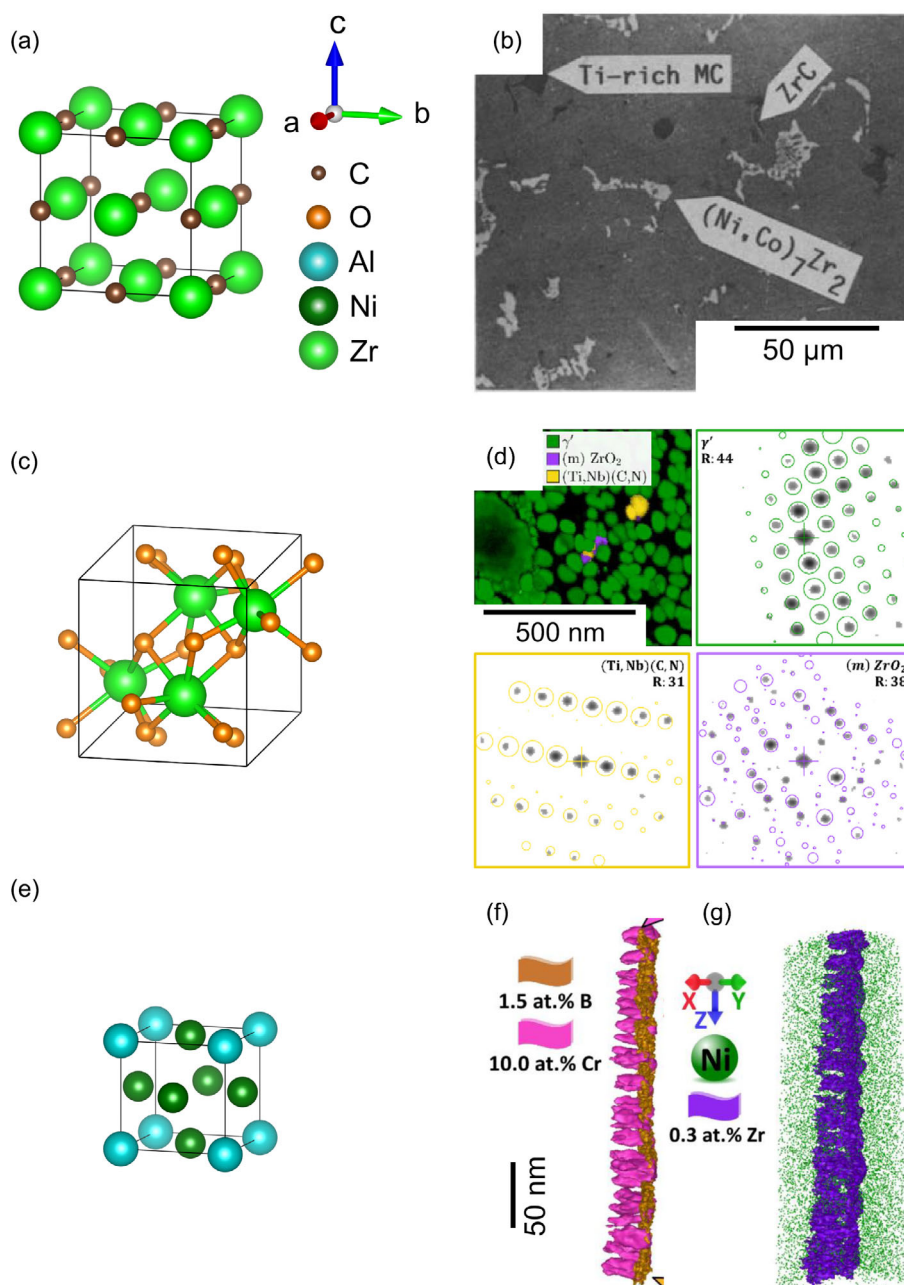


**Figure 7.** a) Unit cell of B1-ordered ZrC,<sup>[168]</sup> b) SEM micrograph of MC and ZrC in IN100. Adapted with permission.<sup>[169]</sup> Copyright 1986, Elsevier. c) Unit cell of C43 ordered *m*-ZrO<sub>2</sub>,<sup>[170]</sup> d) crystallographic phase map of  $\gamma'$  precipitates, (Ti,Nb)(C,N), and *m*-ZrO<sub>2</sub> in AD730. Adapted under the terms of the CC BY 4.0 license.<sup>[111]</sup> Copyright 2021, Elsevier. e) Unit cell of L1<sub>2</sub> ordered (Ni,Zr)<sub>3</sub>(Al,Ti)  $\gamma'$  precipitates,<sup>[171]</sup> f) atom probe reconstruction of nanoscale GB- $\gamma'$  enriched in Zr in AD730. Adapted with permission.<sup>[64]</sup> Copyright 2021, Elsevier.

**Table 6.** Overview of three commonly observed Zr-rich precipitates in polycrystalline Ni-based superalloys.

Phase	Space group	Crystallographic parameters	Structure	References
ZrC	F m -3 m (225)	$a = 0.467 \text{ nm}$	B1 (Ti,Zr)C	[168]
$m\text{-ZrO}_2$	P 1 2 1 /c 1 (14)	$a = 0.513 \text{ nm}, b = 0.520 \text{ nm}, c = 0.531 \text{ nm}$ $\alpha = \gamma = 90^\circ, \beta = 80.82^\circ$	C43 ZrO <sub>2</sub>	[170]
$\gamma'$ precipitates	P m -3 m (221)	$a = 0.357 \text{ nm}$	L1 <sub>2</sub> (Ni,Zr) <sub>3</sub> (Al,Ti)	[171]

**Table 7.** Overview of common commercial cast and wrought Ni-based superalloys.<sup>[12,172–174]</sup> Contents of major alloying elements are comparable, differences are dominated by C, B, and others.

Superalloy	wt%									
	Ni	Cr	Co	Mo	Ti	Al	Fe	C	B	Others
Waspaloy		19	13.5	4.3	3.0	1.4	2.0	0.070	0.006	0.09 Zr
René 41		19	11	10	3.1	1.5	5.0	0.090	0.006	–
René 65		16	13	4	3.7	2.1	1.0	–	0.016	4.0 W, 0.7 Nb, 0.05 Zr
Haynes® 263®	Bal.	20	20	6	2.4	0.6	0.7	0.060	0.050	–
Haynes® 282®		20	10	8.5	2.1	1.5	1.5	0.060	0.005	–
Udimet 700		15	18.5	5	3.4	4.3	–	0.080	0.030	–
Udimet 720		18	14.8	3	5	2.5	–	0.030	0.030	0.03 Zr, 1.25 W
RR1000		15	18.5	5	3.6	3.0	–	0.027	0.015	2.0 Ta, 0.06 Zr, 0.5 Hf

noncommercial prototype superalloys. C, B, and “others” represent the microalloying additions. For example, Waspaloy, René 65, and RR1000 contain considerable amounts of Zr additions. Comparing the C contents of Udimet 720 and René 65 versus Udimet 700 and René 41 shows considerable differences in Zr and B additions. Low B contents may be found in Haynes 282, while comparatively high B contents may be found in Haynes 263. As outlined in the sections earlier, microalloying elements may be necessary to mitigate hot workability, high-temperature strength, and creep strength and more recently developed grades such as RR1000 and René 65 exhibit remarkably complex compositions.

A comparison between Udimet 720 and Udimet 720LI allows to further rationalize the roles of B and C. Both superalloys contain  $\gamma'$  precipitates, MC, and  $M_{23}C_6$  carbides, and  $M_3B_2$  borides have been reported occasionally.<sup>[175,176]</sup> Cr, C, and B are reduced in Udimet 720LI to remove carbide and boride stringers and thus improve hot workability and high-temperature strength.<sup>[176,177]</sup> However, C and B additions in PM Udimet 720 can improve the creep rupture life.<sup>[178]</sup> Considerable compositional variations between superalloys developed in different geographic regions reflect versatile applications and processing routes. Large-scale power generation applications favor cast and wrought processable superalloys, such as GH4141 (sim. René 41) with somewhat more B, C, and Zr additions.<sup>[12,179]</sup> High-performance gas turbine engines require PM superalloys, such as EP741NP developed in Russia, with low C contents and additional carbide or oxide formers instead.<sup>[180–182]</sup>

Table 1, Table 3, and Table 5 highlight the unique properties of B, C, and Zr in GB segregation and precipitation. However, information on the combined impact of microalloying elements on the mechanical properties of Ni-based superalloys is more sparse. Benhadad et al.<sup>[183]</sup> showed competitive segregation

between C and B and C and P in a 718-type superalloy. The complexity is highlighted by Alam et al.,<sup>[184]</sup> providing evidence of C clustering instead of site competition in a similar superalloy. Detrois et al.<sup>[56]</sup> showed that Si contamination in Ni-based superalloys could offset the cohesive benefit of B microalloying. Moreover, different Zr additions, e.g., in Waspaloy and RR1000, make recycling challenging when primary materials and scrap from various other superalloys are combined.<sup>[17,18]</sup> It is often economically unviable or even thermodynamically impossible to remove additions in such low quantities.<sup>[2,18]</sup>

A more generalized understanding of GB segregation is therefore helpful. Formulations on GB segregation are compiled by Flewitt & Wild.<sup>[32]</sup> Equilibrium segregation is driven by a reduction of the interfacial-free energy.<sup>[185]</sup> In binary systems, the amount of solutes is estimated using the Langmuir–McLean approach,<sup>[186,187]</sup> or its expanded form by Seah & Hondros.<sup>[188]</sup> The maximum excess solute concentration has been derived by Cahn & Hilliard.<sup>[189]</sup> However, in compositionally complex alloys, this may not provide satisfying results. Instead, a regular ternary model consisting of metallic alloying elements  $M$  and impurities  $I$  within a matrix can be assumed.<sup>[190]</sup> Competitive segregation of  $M$  and  $I$  sharing the same sites at a GB yields Equation (4).<sup>[191]</sup>

$$\frac{X_i^\Phi}{1 - X_I^\Phi - X_M^\Phi} = X_i^B \exp\left(\frac{\Delta G_i}{RT}\right) \quad (4)$$

Here,  $X_i^\Phi$  and  $X_i^B$  are concentrations of species  $i = M$  or  $I$  at the GB  $\Phi$  or in bulk  $B$ , respectively.  $R$  and  $T$  refer to the universal gas constant and absolute temperature, respectively.  $\Delta G_I = \Delta G_I^0 + \alpha' X_M^\Phi$  and  $\Delta G_M = \Delta G_M^0 + \alpha' X_I^\Phi$  are then defined with  $\alpha$  as preferential interaction coefficient. Noncompetitive segregation of  $M$  and  $I$  occupying different sites at a GB yields Equation (5).<sup>[192]</sup>

$$\frac{Y_i^\phi}{1 - Y_i^\phi} = X_i^B \exp\left(\frac{\Delta G_i}{RT}\right) \quad (5)$$

Here,  $Y_i^\phi$  represents the concentrations of  $i = M$  or  $I$  in their respective sites. Saturation  $\phi$  at a GB is achieved when  $Y_I^\phi = Y_M^\phi$ . With  $b = X_I^\phi$  and  $a = X_M^\phi$ , and  $\beta$  as preferential interaction coefficient yields  $\Delta G_I = \Delta G_I^0 + \beta' Y_M^\phi/b$  and  $\Delta G_M = \Delta G_M^0 + \beta' Y_I^\phi/a$ . Attractive interaction between  $M$  and  $I$  is described by  $\alpha$  or  $\beta > 0$ . As result,  $M$  and  $I$  may promote GB segregation of each other, such as  $M$  attracts  $I$  to GBs, or vice versa.

Indeed, numerous examples for complex GB co-segregation can be found in experimental and numerical studies. For example, S and P have been found to attract Mo and Nb toward GBs in Inconel 718.<sup>[193]</sup> In particular, the co-segregation of P and Mo was later confirmed by studies on 718 Plus.<sup>[194]</sup> More recently, CALPHAD (calculation of phase diagrams) by Wang & Kamachali<sup>[195]</sup> quantitatively demonstrated the temperature dependence of GB co-segregation in highly alloyed systems. First-principles calculations by Xue et al.<sup>[159]</sup> could show that GB segregation of Zr also result in the co-segregation of Zr–Ta, Zr–Re, and Zr–Cu in superalloys.

Enthalpy and entropy of GB segregation are determined using bond-breaking models,<sup>[196,197]</sup> while elastic strains are derived from the atomic mismatch.<sup>[186,198]</sup> More recent formulations of heat of formation, surface energy, and heat of segregation are provided by Bozzolo et al.<sup>[199–201]</sup> Following Fick's diffusion equations,<sup>[187]</sup> GB segregation concentration profiles take the shape of an error function if kinetics are considered.<sup>[32]</sup> Estimations are improved by using the finite difference method or considering contribution from volume diffusion, dislocation pipe diffusion, and dislocation enrichment.<sup>[202,203]</sup>

Nonequilibrium segregation may be divided into thermally induced, neutron irradiation-induced, and stress-driven segregation.<sup>[32]</sup> However, this is less relevant during cast and wrought processing due to thermo-mechanical profiles much closer to equilibrium conditions.<sup>[204,205]</sup> Thermally induced non-equilibrium segregation is the result of solute-vacancy complexes

migrating toward GBs acting as vacancy sinks. This depends on vacancy energy, coordination number, vacancy-solute interaction energy,<sup>[206,207]</sup> as well as atomic mismatch.<sup>[208]</sup> Stress-driven non-equilibrium segregation is the result of vacancies generated at  $>0.4 T_m$  (with  $T_m$  as homologous melting temperature) may limit GB segregation by improving solubility of solutes in the grain interior.<sup>[209,210]</sup> However, this is of particular interest during welding and post-weld heat treatments.<sup>[211]</sup>

## 5.2. Solid-State Phase Transformations

Comprehensive overviews of aerospace materials, their properties, and processing are provided by Sims et al.,<sup>[129]</sup> Donachie & Donachie,<sup>[6]</sup> Campbell,<sup>[5]</sup> and Reed.<sup>[4]</sup> B, C, and Zr can result in the precipitation of borides ( $M_2B$ ,  $M_3B_2$ , and  $M_5B_3$ ), carbides (MC,  $M_6C$ ,  $M_{23}C_6$ , and  $M_7C_3$ ), or other Zr-rich inclusions (ZrC,  $ZrO_2$ , and  $ZrB_2$ ). Geometrically close-packed (GCP) phases, such as  $\gamma'$ ,  $\gamma''$ ,  $\eta$ , and  $\delta$ , are embedded in the  $\gamma$ -matrix. Their stability is determined by Ni, Al, Ti, and Nb in each superalloy, whereas  $\gamma'$  and  $\gamma''$  precipitates provide high-temperature strength.<sup>[151,177,212,213]</sup>  $\eta$  and  $\delta$  are similar in composition and structure, but contribute to Zener–Smith pinning and thus grain size control.<sup>[214,215]</sup> TCP phases are formed by Co, Cr, Mo, and W. Due to their brittleness, they are detrimental to mechanical properties. Examples are  $\sigma$ ,  $\mu$ , and Laves phases.<sup>[67,216–218]</sup> Fe and Co predominantly remain in solid solution in the  $\gamma$ -matrix, and their impact on solid solution strengthening is estimated using Gypen–Deruyttere model.<sup>[219,220]</sup> Furthermore, carbide clusters may act as void nucleation sites and excessive porosity can promote forge cracking.<sup>[31,41,47,59]</sup>

Figure 8 presents an empirical study of microstructural features influenced by B, C, and Zr microalloying additions. It is classified into carbides (e.g., MC, or  $M_6C$ , or  $M_{23}C_6$ ), borides (e.g.,  $M_2B$ , or  $M_3B_2$ , or  $M_5B_3$ ), or both. It must be noted that processing conditions, characterization methods, and major alloying elements are not considered and may limit the wider applicability of these diagrams. A more intuitive and interactive representation is provided in the supporting material as a 3D scatter plot. Figure 8a reveals two domains in the C and B contents. Carbides

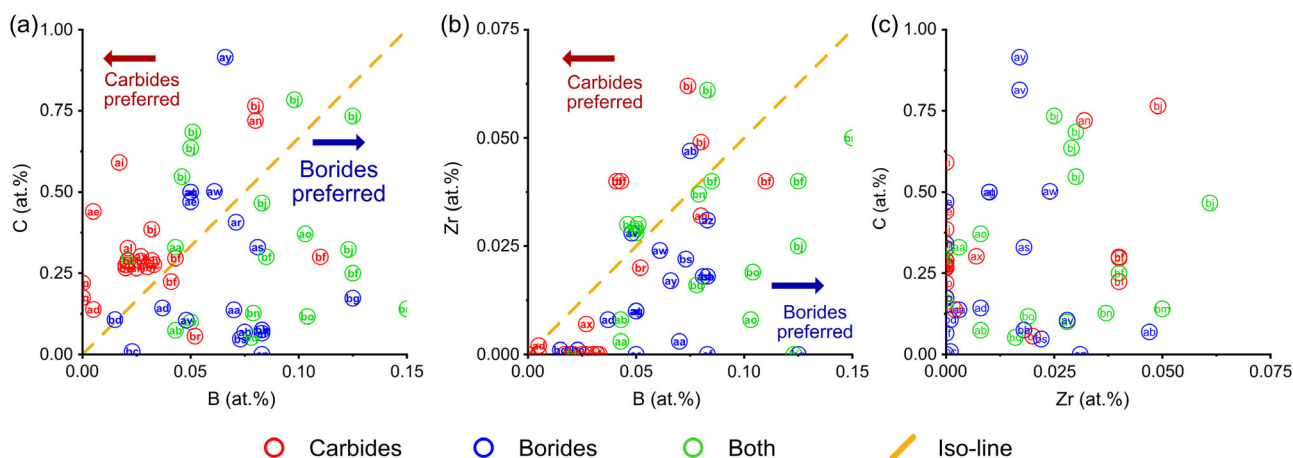


**Figure 8.** Preferences for carbide and boride formation, depending on a) C and B, b) Zr and B, and c) C and Zr contents.<sup>[12,26–28,40,47,48,54,56,57,63–65,80,81,104,106,108,111,137,143,221–224]</sup> For a more intuitive representation and a table of the used references, readers are referred to the supporting information.

are predominantly preferred above the isoline, below which borides and both, carbides and borides, are preferred. The formation of borides with increasing B content appears trivial; however, it is remarkable that a similar trend is followed by various grades of superalloys. A minimal amount of B may be beneficial due to GB segregation<sup>[48,77–81]</sup> as well as the capability of some carbides to dissolve small amounts of B.<sup>[26,221]</sup> Figure 8b reveals similar domains between Zr and B contents. Above the isoline, carbides are preferred, below which borides are preferred. This is due to the capability of Zr to form or dissolve in carbides.<sup>[148,152]</sup> With increasing B concentration, borides, or both, carbides and borides, are promoted. Figure 8c shows the C and Zr contents and no clear trend in the preference for carbide or boride formation. This may be due to the capability of Zr to promote the formation or dissolve in GB precipitates.<sup>[111,152]</sup> However, other elements such as Cr and Mo promoting the formation of carbides should be considered as well.

### 5.3. Processability and Properties

Most studies focus on the roles of B, C, and Zr in creep resistance,<sup>[56,63,64]</sup> fatigue crack growth,<sup>[85,245,246]</sup> casting,<sup>[9,11,150]</sup> and welding<sup>[107,183,247]</sup> or AM processes.<sup>[57,62,183,248,249]</sup> Fewer studies provide in-depth knowledge about these elements during cast and wrought processing.<sup>[26,27,40,222]</sup>

Fluidity improvements are recorded for B and C during casting and (re-)melting.<sup>[9,115]</sup> The formation of detrimental eutectics, such as  $\gamma + \gamma'$ , is most severe for Zr, B, or combined.<sup>[10,11,115,116,155]</sup> Zr and B both hinder solute exchange

between liquid and solid phases, and Zr promotes the formation of  $\gamma'$  precipitates.<sup>[10,11,76]</sup> Thus, homogenization treatments must be adjusted before hot working can be carried out. Solid-state micro-segregation of B, C, and Zr, and impurities may be competitive processes.<sup>[37,56,96,183]</sup> For example, B may replace P at GBs or O at phase boundaries and offset their embrittling effect.<sup>[37,96]</sup> Alloying elements such as Mo and Cr may also compete to segregate to GBs.<sup>[52,57]</sup> Their segregation can precede the formation of GB carbides or borides.<sup>[42,49]</sup> However, detailed knowledge of these mechanisms remains lacking. Micro-mechanical testing of individual GBs<sup>[250,251]</sup> correlates well with first-principles calculations<sup>[36,38,95,96]</sup> assigning B a positive effect on GB strengthening. GB serrations introduced by GB precipitates can improve the ductility,<sup>[39]</sup> but void formation around GB carbides can be detrimental.<sup>[252]</sup> However, hot working conditions are much more difficult to reproduce with in situ experiments, and thus, fewer studies are available to date.

GB co-precipitation results in complex GB microstructures as illustrated in **Figure 9**. GB- $\gamma'$ , carbides, and borides can decorate GBs concurrently and thus introduce various new interfaces. Some examples are  $\gamma$ -matrix/GB- $\gamma'$ ,  $\gamma$ -matrix/carbide,  $\gamma$ -matrix/boride, GB- $\gamma'$ /carbide, and GB- $\gamma'$ /boride phase boundaries. However, local composition and mechanical properties of these interfaces remain widely unexplored. A consistent understanding of these microstructural features and their properties across different superalloy grades is essential. This requires additional studies on the roles of GB segregation and (co-)precipitation in cast and wrought Ni-based superalloys.

Continuing to focus on GB- $\gamma'$ , GB-carbides, and GB-borides in Figure 9, their reported chemical and physical properties remain

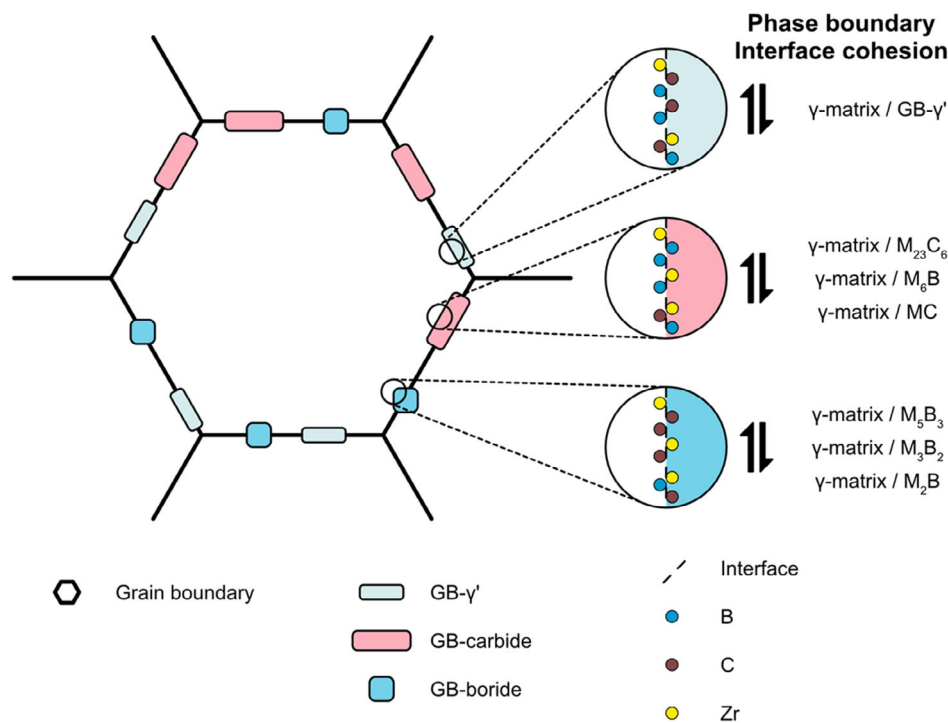


**Figure 9.** Microstructural model of various potential phases and interfaces in cast and wrought Ni-based superalloys. GB- $\gamma'$ , GB-carbides (MC,  $M_6C$ ,  $M_{23}C_6$ ), and GB-borides ( $M_2B$ ,  $M_3B_2$ , and  $M_5B_3$ ) result in complex GB microstructures, and their interfaces may impact segregation of B, C, and Zr. The interface cohesion is determined by local composition of their respective interfaces to the  $\gamma$ -matrix.

controversial. As superalloy composition and processing conditions affect phase compositions,<sup>[253,254]</sup> reliable phase identification, e.g., between Mo-rich  $M_6C$ ,  $M_3B_2$ , and  $M_2B$ , is challenging.<sup>[80,228,255,256]</sup> Some local mechanical properties are reported for  $\gamma'$  precipitates, intragranular carbides, or the  $\delta$ -phase in superalloys,<sup>[257–260]</sup> and are invaluable for precise mechanical modeling.<sup>[261–263]</sup> Quantitative experimental methods<sup>[72,157,158,264–267]</sup> and data analysis approaches<sup>[88,89,184,268]</sup> exist for GB segregation. However, little to no quantitative information is reported for the local composition of phase boundaries in the proximity of GBs. First-principles calculations to verify local electronic structures of  $\gamma$ -matrix/GB- $\gamma'$ ,  $\gamma$ -matrix/GB-carbide, or  $\gamma$ -matrix/GB-boride are sparse.<sup>[36,37]</sup> However, properties of these phase boundaries are important to assess GB strength. Various phases decorating GBs introduce additional interfaces in the proximity of GBs. As the composition of GB- $\gamma'$ , carbides, and borides vary considerably, their interfaces have the potential to exhibit different types and degrees of segregation on the atomic scale. The development of experimental and data analysis approaches to address these shortcomings may not only be applicable to cast and wrought Ni-based superalloys but may be employed to solve similar challenges in Fe-based and Al alloys.<sup>[234–241]</sup>

## 6. Conclusions

### 6.1. State of Knowledge

Processing–microstructure–property relationships in cast and wrought Ni-based superalloys with B, C, and Zr microalloying additions are dominated by GB segregation, precipitation, and complex co-precipitation/segregation phenomena.

GB segregation of B can be considered as beneficial to GB strength and cohesion, based on experimental and first-principles calculations. Compared to C and Zr, B exhibits the strongest affinity toward GB segregation. However, excessive GB segregation of B may result in the precipitation of borides, such as  $M_2B$ ,  $M_3B_2$ , or  $M_5B_3$ . Cr-rich  $M_5B_3$  can improve ductility via GB serrations, while Mo-rich  $M_3B_2$  is associated with detrimental GB incipient melting and eutectic formation. Less frequently observed is  $M_2B$  that can be Cr or Mo-rich and may exhibit detrimental or beneficial effects to mechanical properties.

GB segregation of C is considered to have no significantly detrimental impact on GB strength and cohesion. Compared to B and Zr, its relative affinity to GB segregation is lower. Thus, C predominantly results in the precipitation of carbides, such as MC,  $M_6C$ , or  $M_{23}C_6$ . MC carbides exhibit opposing properties: GB pinning at elevated temperatures may be beneficial for grain size control. However, this can also result in inhomogeneous grain size distributions or act as crack nucleation sites. Mo-rich  $M_6C$  forms discrete GB precipitates that are less brittle than MC or  $M_{23}C_6$ . They are the most suitable in grain growth control but are observed in Mo- or W-rich Ni-based superalloys, such as René 41 and Haynes 282. Cr-rich  $M_{23}C_6$  are more commonly observed than  $M_6C$  and tend to form near-continuous films at GBs. Beneficial as well as detrimental properties are reported and ascribed to their detailed morphology.

GB segregation of Zr is often expected to impact GB strength and cohesion similarly to B. However, experimental results reveal much more complex mechanisms. The formation of eutectics and promotion of GB- $\gamma'$  precipitates may be detrimental to ductility and processability. However, Zr may also refine carbides, such as MC to mitigate their brittleness. Zr may be used for “gettering” of detrimental tramp elements, such as O, S, and P. Its strong affinity toward O promotes the formation of  $ZrO_2$  that may be a nucleation site for carbides, borides, and  $\gamma'$  precipitates.

Challenges in future cast and wrought Ni-based superalloy design center around finding compromises in superalloy complexity, processability, and recyclability. Here, more detailed characterization of structure and composition of (co-)precipitates in the proximity of GBs is required. The interaction of co-precipitation and segregation across phase boundaries is less well documented and requires for a more complete understanding of the microstructure–properties relationships in advanced cast and wrought Ni-based superalloys.

### 6.2. Future Prospects

In the foreseeable future, cast and wrought Ni-based superalloys will likely remain the workhorse for high-temperature components in gas turbine engines. In their ongoing development, the following should be considered:

**Compositional complexity:** Mitigating high-temperature strength and processability via microalloying elements B, C, and Zr adds to the complexity of Ni-based superalloys. An advanced understanding of even more complex microstructure–property relationships across different superalloy grades is therefore required to optimize GB segregation and precipitation.

**Recycling:** Improving recycling rates requires the combination of scraps of different superalloy grades, such as Waspaloy, René 41, and Haynes 282 with varying contents of B, C, and Zr. However, controlled recovery and isolation of microalloying elements are economically challenging. Enabling the recycling of a wider range of end-of-life products and scraps requires the advanced understanding of the roles of these elements across different superalloys.

Therefore, future work needs to address challenges in GB segregation and precipitation in cast and wrought Ni-based superalloys.

**Local composition of phase boundaries:** Crystallography and local composition of GBs with  $\gamma$ -matrix/ $\gamma$ -matrix interfaces are challenges in current research. Most Ni-based superalloys exhibit highly complex GB microstructures with co-precipitating phases and added complexity in terms of segregation at various phase boundaries. Quantifying and modeling the local composition of such phase boundaries is required for a more detailed understanding of the mechanical properties during manufacturing and in-service of cast and wrought Ni-based superalloys.

**Characterization techniques:** While atom probe microscopy is suitable to determine the local composition of interfaces, captured volumes are limited. Enabling larger volumes can improve statistically relevant measurements. High-resolution

TEM imaging and local compositional mapping may be advantageous due to structural and compositional information captured from the same specimen. However, quantification of light elements, such as B and C remain challenging.

Data analysis techniques: Advances in interfacial excess mapping or employing machine learning reveal new details about GB segregation. However, this should be extended from  $\gamma$ -matrix/ $\gamma$ -matrix interfaces toward phase boundaries, e.g.,  $\gamma$ -matrix/carbides or  $\gamma$ -matrix/borides.

Characterization of composition and structure of GB precipitates are more matured. However, future work should address the following current shortcomings:

Compositional characterization: Quantitative high-resolution characterization is challenging but necessary for reliable phase identification. While structure and composition of some borides and carbides can be similar, their mechanical properties and high-temperature stability may vary considerably.

Mechanical properties: The impact of  $\gamma'$  precipitates, carbides and borides on the mechanical properties should be explored in more detail. That includes their roles in strengthening and crack initiation in the vicinity of GBs during cast and wrought processing.

## Acknowledgements

The authors thank Prof. Ernst Kozeschnik, Prof. Peter Felfer, Dr. Nima Haghdadadi, and Mr. Han Lin Mai for their fruitful discussions. This research was funded by the Australian Research Council (ARC) Linkage grants LP190101169 and LP180100144. S.P. was further supported by UNSW Scientia Fellowship schemes. R.B. thanks Georgia and Pietro Bergamaschi for personal and financial support.

Open access publishing facilitated by University of New South Wales, as part of the Wiley - University of New South Wales agreement via the Council of Australian University Librarians.

## Conflict of Interest

The authors declare no conflict of interest.

## Data Availability Statement

The data that supports the findings of this study are available in the supplementary material of this article.

## Keywords

cast and wrought, grain boundary, microalloying, Ni-based superalloy, precipitation, processability, segregation

Received: October 19, 2022

Revised: November 28, 2022

Published online:

- [1] M. J. Eckelman, *Resour. Conserv. Recycl.* **2010**, *54*, 256.  
 [2] G. M. Mudd, S. M. Jowitt, *Econ. Geol.* **2014**, *109*, 1813.  
 [3] A. Kracke, in *7th Int. Symp. on Superalloy 718 and Derivatives (2010)*, John Wiley & Sons, Inc. Hoboken, NJ **2010**, p. 13.

- [4] R. C. Reed, in *The Superalloys Fundamentals and Applications*, Cambridge University Press, Cambridge, UK **2006**.  
 [5] F. C. Campbell, in *Manufacturing Technology for Aerospace Structural Materials*, Elsevier, Amsterdam **2006**.  
 [6] M. J. Donachie, S. J. Donachie, in *Superalloys: A Technical Guide*, ASM International, Materials Park, OH **2002**.  
 [7] C. L. Briant, R. P. Messmer, *Acta Metall.* **1982**, *30*, 1811.  
 [8] J. M. Walsh, B. H. Rear, *MTA* **1975**, *6*, 226.  
 [9] Z. Jie, J. Zhang, T. Huang, H. Su, Y. Zhang, L. Liu, H. Fu, *J. Mater. Res.* **2016**, *31*, 3557.  
 [10] H. Wang, J. Yang, J. Meng, S. Ci, Y. Yang, N. Sheng, Y. Zhou, X. Sun, *J. Alloys Compd.* **2021**, *860*, 157929.  
 [11] J. Grodzki, N. Hartmann, R. Rettig, E. Affeldt, R. F. Singer, *Metall. Mater. Trans. A* **2016**, *47*, 2914.  
 [12] L. Pike, *Superalloys* **2008**, 191.  
 [13] M. C. Hardy, M. Detrouis, E. T. McDevitt, C. Argyrakakis, V. Saraf, P. D. Jablonski, J. A. Hawk, R. C. Buckingham, H. S. Kitaguchi, S. Tin, *Metall. Mater. Trans. A* **2020**, *51*, 2626.  
 [14] M. T. Schobeiri, in *Gas Turbine Design, Components and System Design Integration*, Springer International Publishing, Cham **2019**, p. 33.  
 [15] A. Sato, M. Imamura, T. Fujimura, *IHI Eng. Rev.* **2014**, *47*, 23.  
 [16] J. A. Muldoon, B. G. Harvey, *ChemSusChem* **2020**, *13*, 5777.  
 [17] T. E. Graedel, E. M. Harper, N. T. Nassar, B. K. Reck, *Proc. Natl. Acad. Sci. USA* **2015**, *112*, 6295.  
 [18] B. K. Reck, T. E. Graedel, *Science* **2012**, *337*, 690.  
 [19] V. V. Sidorov, D. N. Petrov, O. M. Kosenkov, *Russ. Metall.* **2020**, *2020*, 692.  
 [20] L. Whitmore, M. R. Ahmadi, L. Guetaz, H. Leitner, E. Povoden-Karadeniz, M. Stockinger, E. Kozeschnik, *Mater. Sci. Eng. A* **2014**, *610*, 39.  
 [21] M. R. Ahmadi, L. Whitmore, E. Povoden-Karadeniz, M. Stockinger, A. Falahati, E. Kozeschnik, *Adv. Mater. Res.* **2014**, *922*, 7.  
 [22] A. J. Goodfellow, *Mater. Sci. Technol.* **2018**, *34*, 1793.  
 [23] H. U. Hong, I. S. Kim, B. G. Choi, M. Y. Kim, C. Y. Jo, *Mater. Sci. Eng. A* **2009**, *517*, 125.  
 [24] D. Furrer, *Scr. Mater.* **1999**, *40*, 1215.  
 [25] C. L. Qiu, P. Andrews, *Mater. Character.* **2013**, *76*, 28.  
 [26] R. Buerstmayr, F. Theska, R. Webster, M. Lison-Pick, S. Primig, *Mater. Character.* **2021**, *178*, 111250.  
 [27] C. Joseph, M. Hörnqvist, R. Brommesson, C. Persson, in *Superalloys 2016* (Eds: M. Hardy, E. Huron, U. Glatzel, B. Griffin, B. Lewis, C. Rae, V. Seetharaman, S. Tin), John Wiley & Sons, Inc., Hoboken, NJ **2016**, p. 523.  
 [28] X. B. Hu, Y. L. Zhu, X. L. Ma, *Acta Mater.* **2014**, *68*, 70.  
 [29] X. B. Hu, H. Y. Niu, X. L. Ma, A. R. Oganov, C. A. J. Fisher, N. C. Sheng, J. D. Liu, T. Jin, X. F. Sun, J. F. Liu, Y. Ikuhara, *Acta Mater.* **2018**, *149*, 274.  
 [30] X. B. Hu, Y. L. Zhu, N. C. Sheng, X. L. Ma, *Sci. Rep.* **2015**, *4*, 7367.  
 [31] S. Yang, S. Yang, J. Qu, J. Du, Y. Gu, P. Zhao, N. Wang, *J. Iron Steel Res. Int.* **2021**, *28*, 921.  
 [32] P. E. J. Flewitt, R. K. Wild, in *Grain Boundaries: Their Microstructure and Chemistry*, J. Wiley, Chichester, England **2001**.  
 [33] D. Y. Lee, E. V. Barrera, J. P. Stark, H. L. Marcus, *MTA* **1984**, *15*, 1415.  
 [34] R. T. Holt, W. Wallace, *Int. Metals Rev.* **1976**, *21*, 1.  
 [35] S. Etris, Y. Fiorini, K. Lieb, I. Moore, A. Batik, W. Wallace, R. Holt, E. Whelan, *J. Test. Eval.* **1975**, *3*, 113.  
 [36] S. Sanyal, U. V. Waghmare, P. R. Subramanian, M. F. X. Gigliotti, *Appl. Phys. Lett.* **2008**, *93*, 223113.  
 [37] S. Sanyal, U. V. Waghmare, T. Hanlon, E. Hall, P. R. Subramanian, M. F. X. Gigliotti, in *Superalloys 2012: 12th International Symposium on Superalloys*, **2012**, p. 531.  
 [38] V. I. Razumovskiy, A. Y. Lozovoi, I. M. Razumovskii, *Acta Mater.* **2015**, *82*, 369.

- [39] P. Kontis, E. Alabort, D. Barba, D. M. Collins, A. J. Wilkinson, R. C. Reed, *Acta Mater.* **2017**, *124*, 489.
- [40] F. Theska, R. Buerstmayr, H. Liu, M. Lison-Pick, S. R. Street, S. Primig, *Mater. Character.* **2022**, *187*, 111881.
- [41] Y. Han, X. Xue, T. Zhang, R. Hu, J. Li, *Mater. Sci. Eng. A* **2016**, *667*, 391.
- [42] R. Dong, J. Li, T. Zhang, R. Hu, H. Kou, *Mater. Character.* **2016**, *122*, 189.
- [43] V. I. Razumovskiy, A. Y. Lozovoi, I. M. Razumovskii, A. V. Ruban, *AMR* **2011**, *278*, 192.
- [44] V. I. Razumovskiy, A. Y. Lozovoi, I. M. Razumovskii, *Acta Mater.* **2016**, *106*, 401.
- [45] D. M. Collins, B. D. Conduit, H. J. Stone, M. C. Hardy, G. J. Conduit, R. J. Mitchell, *Acta Mater.* **2013**, *61*, 3378.
- [46] C. Liu, F. Liu, L. Huang, L. Jiang, *Trans. Nonferrous Metals Soc. China* **2014**, *24*, 2544.
- [47] R. Hu, G. Bai, J. Li, J. Zhang, T. Zhang, H. Fu, *Mater. Sci. Eng. A* **2012**, *548*, 83.
- [48] O. A. Ojo, H. R. Zhang, *Metall. Mater. Trans. A* **2008**, *39*, 2799.
- [49] H. U. Hong, I. S. Kim, B. G. Choi, Y. S. Yoo, C. Y. Jo, **2012**, *Superalloys 2012: 12th International Symposium on Superalloys*, 53–61.
- [50] W. J. Boesch, H. B. Canada, *JOM* **1968**, *20*, 46.
- [51] M. R. Jahangiri, S. M. A. Boutorabi, H. Arabi, *Mater. Sci. Technol.* **2012**, *28*, 1402.
- [52] D. Tytko, P.-P. Choi, J. Klöwer, A. Kostka, G. Inden, D. Raabe, *Acta Mater.* **2012**, *60*, 1731.
- [53] G. Bai, J. Li, R. Hu, Z. Tang, X. Xue, H. Fu, *Mater. Sci. Eng. A* **2011**, *528*, 1974.
- [54] P. Kontis, A. Kostka, D. Raabe, B. Gault, *Acta Mater.* **2019**, *166*, 158.
- [55] L. Lilensten, A. Kostka, S. Lartigue-Korinek, B. Gault, S. Tin, S. Antonov, P. Kontis, *JOM* **2021**, *73*, 2293.
- [56] M. Detrois, Z. Pei, T. Liu, J. D. Poplawsky, M. C. Gao, P. D. Jablonski, J. A. Hawk, *Scr. Mater.* **2021**, *201*, 113971.
- [57] P. Kontis, E. Chauvet, Z. Peng, J. He, A. K. da Silva, D. Raabe, C. Tassin, J.-J. Blandin, S. Abed, R. Dendievel, B. Gault, G. Martin, *Acta Mater.* **2019**, *177*, 209.
- [58] J. Zhang, in *Superalloys 2004 (Tenth Int. Symp.)*, TMS (The Minerals, Metal & Materials Society) **2004**, p. 727.
- [59] D. Texier, J.-C. Stinville, M. P. Echlin, S. Pierret, P. Villechaise, T. M. Pollock, J. Cormier, *Acta Mater.* **2019**, *165*, 241.
- [60] M. P. Haines, V. V. Rielli, S. Primig, N. Haghdadi, *J. Mater. Sci.*, *57*, 14135.
- [61] A. Chamanfar, M. Jahazi, J. Cormier, *Metall. Mater. Trans. A* **2015**, *46*, 1639.
- [62] T. Saju, M. Velu, *Mater. Today Proc.* **2021**, *46*, 7161.
- [63] P. Kontis, H. A. M. Yusof, S. Pedrazzini, M. Danaie, K. L. Moore, P. A. J. Bagot, M. P. Moody, C. R. M. Grovenor, R. C. Reed, *Acta Mater.* **2016**, *103*, 688.
- [64] A. Després, S. Antonov, C. Mayer, C. Tassin, J.-J. Blandin, P. Kontis, G. Martin, *ArXiv:2105.08307 [Cond-Mat]* **2021**.
- [65] L. Lilensten, A. Kostka, S. Lartigue-Korinek, S. Antonov, S. Tin, B. Gault, P. Kontis, (Preprint) arXiv:2007.02581, v1, submitted: Jul. **2020**.
- [66] M. Wagih, C. A. Schuh, *Phys. Rev. Lett.* **2022**, *129*, 046102.
- [67] S. Antonov, M. Detrois, D. Isheim, D. Seidman, R. C. Helmink, R. L. Goetz, E. Sun, S. Tin, *Mater. Des.* **2015**, *86*, 649.
- [68] D. Raabe, M. Herbig, S. Sandlöbes, Y. Li, D. Tytko, M. Kuzmina, D. Ponge, P.-P. Choi, *Curr. Opin. Solid State Mater. Sci.* **2014**, *18*, 253.
- [69] J. E. Halpin, R. W. H. Webster, H. Gardner, M. P. Moody, P. A. J. Bagot, D. A. MacLaren, *Ultramicroscopy* **2019**, *202*, 121.
- [70] M. Kühbach, P. Bajaj, H. Zhao, M. H. Çelik, E. A. Jäggle, B. Gault, *NPJ Comput. Mater.* **2021**, *7*, 21.
- [71] L. Huber, R. Hadian, B. Grabowski, J. Neugebauer, *NPJ Comput. Mater.* **2018**, *4*, 64.
- [72] B. Gault, M. P. Moody, J. M. Cairney, S. P. Ringer, in *Atom Probe Microscopy*, Springer New York, New York, NY **2012**.
- [73] D. E. Newbury, N. W. M. Ritchie, *J. Mater. Sci.* **2015**, *50*, 493.
- [74] D.E. Newbury, C. R. Swyt, R. L. Myklebust, *Anal. Chem.* **1995**, *67*, 1866.
- [75] Y. Zhu, J. Cai, N. S. Hosmane, Y. Zhang, in *Fundamentals and Applications of Boron Chemistry* Elsevier, Amsterdam **2022**, p. 1.
- [76] S. A. Hosseini, S. M. Abbasi, K. Z. Madar, *J. Mater. Eng. Perform.* **2018**, *27*, 2815.
- [77] K. I. Portnoi, V. M. Romashov, *Powder Metall. Met. Ceram.* **1972**, *11*, 378.
- [78] O. Teppa, P. Taskinen, *Mater. Sci. Technol.* **1993**, *9*, 205.
- [79] H. U. Hong, I. S. Kim, B. G. Choi, Y. S. Yoo, C. Y. Jo, *Metall. Mater. Trans. A* **2012**, *43*, 173.
- [80] D. Blavette, E. Cadel, C. Pareige, B. Deconihout, P. Caron, *Microsc. Microanal.* **2007**, *13*, 464.
- [81] E. Cadel, D. Lemarchand, S. Chambrelaud, D. Blavette, *Acta Mater.* **2002**, *50*, 957.
- [82] R. F. Decker, J. P. Rowe, J. W. Freeman, Boron and Zirconium from Crucible Refractories in a Complex Heat-Resistant Alloy, The National Advisory Committee for Aeronautics, University of Michigan, Ann Arbor, MI **1958**.
- [83] R. F. Decker, J. W. Freeman, The Mechanism of Beneficial Effects of Boron and Zirconium on Creep-Rupture Properties of a Complex Heat-Resistant Alloy, The National Advisory Committee for Aeronautics, University of Michigan, Ann Arbor, MI **1957**.
- [84] A. H. Cottrell, *Mater. Sci. Technol.* **1991**, *7*, 585.
- [85] S. Floreen, J. M. Davidson, *MTA* **1983**, *14*, 895.
- [86] M. K. Miller, I. M. Anderson, L. M. Pike, D. L. Klarstrom, *Mater. Sci. Eng. A* **2002**, *327*, 89.
- [87] L. Letellier, S. Chambrelaud, P. Duval, D. Blavette, *Appl. Surf. Sci.* **1993**, *67*, 305.
- [88] P. J. Felfer, C. R. Killmore, J. G. Williams, K. R. Carpenter, S. P. Ringer, J. M. Cairney, *Acta Mater.* **2012**, *60*, 5049.
- [89] P. Felfer, B. Scherrer, J. Demeulemeester, W. Vandervorst, J. M. Cairney, *Ultramicroscopy* **2015**, *159*, 438.
- [90] P. Lejcek, in *Grain Boundary Segregation in Metals*, Springer, Berlin, Heidelberg **2010**.
- [91] R. L. Morrison, S. J. Fensin, J. L. W. Carter, *Materialia* **2019**, *7*, 100383.
- [92] R. Kikuchi, S. Suzuki, K. Suzuki, in *Mechanics of Solids, Structures, and Fluids, Vol. 12*, American Society Of Mechanical Engineers, **2020**, V012T12A059.
- [93] M. D. Sangid, H. Sehitoglu, H. J. Maier, T. Niendorf, *Mater. Sci. Eng. A* **2010**, *527*, 7115.
- [94] R. Sperry, A. Harte, J. Quinta da Fonseca, E. R. Homer, R. H. Wagoner, D. T. Fullwood, *Acta Mater.* **2020**, *193*, 229.
- [95] M. Yamaguchi, M. Shiga, H. Kaburaki, *J. Phys.: Condens. Matter* **2004**, *16*, 3933.
- [96] A. S. Ebner, S. Jakob, H. Clemens, R. Pippan, V. Maier-Kiener, S. He, W. Ecker, D. Scheiber, V. I. Razumovskiy, *Acta Mater.* **2021**, *221*, 117354.
- [97] V. P. Gorokhov, B. A. Kolachev, O. A. Parfenova, M. B. Novikova, *Metall. Term. Obrab. Met.* **2003**, *4*, 22.
- [98] X. B. Hu, Y. L. Zhu, X. H. Shao, H. Y. Niu, L. Z. Zhou, X. L. Ma, *Acta Mater.* **2015**, *100*, 64.
- [99] P. Villars, K. Cenzual, SpringerMaterials **2012**, sd\_0251569.
- [100] P. Villars, K. Cenzual, SpringerMaterials **2012**, sd\_0532888.
- [101] P. Villars, K. Cenzual, SpringerMaterials **2012**, sd\_0450616.
- [102] F. Xia, M. D. Sangid, Y. Xiao, X. Gong, T. Gang, L. Chen, W.-W. Xu, *Philos. Mag.* **2020**, *100*, 998.

- [103] M. A. Burke, J. Greggi, G. A. Whitlow, *Scr. Metall.* **1984**, *18*, 91.
- [104] Ł. Rakoczy, B. Rutkowski, M. Grudziński-Rakoczy, R. Cygan, W. Ratuszek, A. Zielińska-Lipiec, *Materials* **2020**, *13*, 4452.
- [105] B. Du, Z. Shi, J. Yang, Z. Chu, C. Cui, X. Sun, L. Sheng, Y. Zheng, *J. Mater. Sci. Technol.* **2016**, *32*, 265.
- [106] H. J. Beattie, *Acta Cryst.* **1958**, *11*, 607.
- [107] J. N. DuPont, J. C. Lippold, S. D. Kiser, in *Welding Metallurgy and Weldability of Nickel-Base Alloys*, John Wiley & Sons, Hoboken, NJ **2009**.
- [108] B. Du, L. Sheng, C. Cui, J. Yang, X. Sun, *Mater. Character.* **2017**, *128*, 109.
- [109] N. N. Greenwood, A. Earnshaw, in *Chemistry of the Elements*, Butterworth-Heinemann, Oxford **1997**.
- [110] P. Delhaes, *Carbon Science and Technology From Energy to Materials*, **2012**.
- [111] A. Després, S. Antonov, C. Mayer, M. Veron, E. F. Rauch, C. Tassin, J.-J. Blandin, P. Kontis, G. Martin, *Addit. Manufact. Lett.* **2021**, *1*, 100011.
- [112] A. Hariharan, L. Lu, J. Risse, A. Kostka, B. Gault, E. A. Jägle, D. Raabe, *Phys. Rev. Mater.* **2019**, *3*, 123602.
- [113] H. Ohtani, M. Hasebe, T. Nishizawa, *ISIJ Int.* **1984**, *24*, 857.
- [114] E. N. Kablov, V. V. Sidorov, D. E. Kablov, P. G. Min, V. E. Rigin, *Russ. Metall.* **2016**, *2016*, 1187.
- [115] L. Liu, T. Jin, N. R. Zhao, Z. H. Wang, X. F. Sun, H. R. Guan, Z. Q. Hu, *Mater. Lett.* **2004**, *58*, 2290.
- [116] W. Zhou, Y. Tian, Q. Tan, S. Qiao, H. Luo, G. Zhu, D. Shu, B. Sun, *Addit. Manufact.* **2022**, *58*, 103016.
- [117] K. A. Al-Jarba, G. E. Fuchs, *Mater. Sci. Eng. A* **2004**, *373*, 255.
- [118] M. F. Henry, Y. S. Yoo, D. Y. Yoon, J. Choi, *Metall. Trans. A* **1993**, *24*, 1733.
- [119] R. J. Mitchell, H. Y. Li, Z. W. Huang, *J. Mater. Process. Technol.* **2009**, *209*, 1011.
- [120] A. K. Koul, R. Thamburaj, *MTA* **1985**, *16*, 17.
- [121] V. V. Atrazhev, S. F. Burlatsky, D. V. Dmitriev, D. Furrer, N. Y. Kuzminykh, I. L. Lomaev, D. L. Novikov, S. Stolz, P. Reynolds, *Metall. Mater. Trans. A* **2020**, *51*, 3648.
- [122] D. B. Williams, E. P. Butler, *Int. Metals Rev.* **1981**, *26*, 153.
- [123] T. M. Pollock, S. Tin, *J. Propuls. Power* **2006**, *22*, 361.
- [124] L. Z. He, Q. Zheng, X. F. Sun, G. C. Hou, H. R. Guan, Z. Q. Hu, *J. Mater. Sci.* **2005**, *40*, 2959.
- [125] R. V. Shakhov, A. A. Ganeev, S. K. Mukhtarov, A. V. Logunov, *LoM* **2018**, *8*, 494.
- [126] G. Zhao, X. Zang, W. Sun, *J. Iron Steel Res. Int.* **2021**, *28*, 98.
- [127] Y. Guan, Y. Liu, Z. Ma, H. Li, H. Yu, *Met. Mater. Int.* **2022**, *28*, 1488.
- [128] G. P. Sabol, R. Stickler, *Phys. Stat. Sol. B* **1969**, *35*, 11.
- [129] C. T. Sims, N. S. Stoloff, W. C. Hagel, editors, *Superalloys II*, Wiley, New York **1987**.
- [130] M. Sundararaman, *Miner. Process. Extr. Metall. Rev.* **2001**, *22*, 681.
- [131] P. Zheng, T. Hou, D. Zhang, X. Liang, H. Lin, G. Jiang, Y. Li, K. Wu, *J. Phys.: Condens. Matter* **2022**, *34*, 285703.
- [132] H. E. Collins, in *Int. Symp. on Structural Stability in Superalloys (1968)*, **1968**, p. 171.
- [133] K. Kuo, *Acta Metall.* **1953**, *1*, 301.
- [134] L. Jiang, X.-X. Ye, Z.-Q. Wang, C. Yu, J.-S. Dong, R. Xie, Z.-J. Li, L. Yan, T.-K. Sham, X.-T. Zhou, A.-M. Li, *J. Alloys Compd.* **2017**, *728*, 917.
- [135] K. Frisk, J. Bratberg, A. Markström, *Calphad* **2005**, *29*, 91.
- [136] M. Liu, W. Zheng, J. Xiang, Z. Song, E. Pu, H. Feng, *J. Iron Steel Res. Int.* **2016**, *23*, 1111.
- [137] L. Jiang, X.-X. Ye, R.-D. Liu, J.-P. Liang, Z.-J. Li, *Mater. Lett.* **2019**, *250*, 167.
- [138] X. Dong, X. Zhang, K. Du, Y. Zhou, T. Jin, H. Ye, *J. Mater. Sci. Technol.* **2012**, *28*, 1031.
- [139] J. Yang, Q. Zheng, X. Sun, H. Guan, Z. Hu, *Mater. Sci. Eng. A* **2006**, *429*, 341.
- [140] P. Villars, K. Cenzual, SpringerMaterials **2012**, sd\_0261188.
- [141] P. Villars, K. Cenzual, SpringerMaterials **2012**, sd\_0540824.
- [142] P. Villars, K. Cenzual, SpringerMaterials **2012**, sd\_0457395.
- [143] C. Joseph, C. Persson, M. Hörnqvist Colliander, *Metall. Mater. Trans. A* **2020**, *51*, 6136.
- [144] X. Qin, X. Yan, D. Huang, X. Zhang, M. Qi, S. Yue, *Metal. Mater. Int.* **2019**, *25*, 1616.
- [145] Y. A. Guo, C. S. Wang, X. Z. Qin, W. H. Lai, L. Z. Zhou, *MSF* **2015**, *816*, 529.
- [146] W. Zhen-wei, Z. Wen-xia, Z. Jing-yi, L. Chang-kui, Z. Zhen, Q. Shi-yu, T. Chun-hu, *Proc. Eng.* **2015**, *99*, 1302.
- [147] W. H. Jiang, X. D. Yao, H. R. Guan, Z. Q. Hu, *Mater. Sci. Technol.* **1999**, *15*, 596.
- [148] C. T. Sims, *JOM* **1966**, *18*, 1119.
- [149] Y. Liu, J. Wang, M. Kang, F. Mao, J. Li, G. Wang, S. He, H. Gao, B. Sun, *Mater. Character.* **2018**, *138*, 174.
- [150] H. Matysiak, M. Zagorska, A. Balkowiec, B. Adamczyk-Cieslak, R. Cygan, J. Cwajna, J. Nawrocki, K. J. Kurzydowski, *J. Mater. Eng. Perform.* **2014**, *23*, 3305.
- [151] A. K. Jena, M. C. Chaturvedi, *J. Mater. Sci.* **1984**, *19*, 3121.
- [152] Y.-L. Tsai, S.-F. Wang, H.-Y. Bor, Y.-F. Hsu, *Mater. Sci. Eng. A* **2014**, *607*, 294.
- [153] S. A. Hosseini, S. M. Abbasi, K. Z. Madar, H. M. K. Yazdi, *Mater. Chem. Phys.* **2018**, *211*, 302.
- [154] C. L. White, J. H. Schneibel, R. A. Padgett, *MTA* **1983**, *14*, 595.
- [155] M. Mostafaei, S. M. Abbasi, *J. Alloys Compd.* **2015**, *648*, 1031.
- [156] J. Zhang, R. F. Singer, *Metall. Mater. Trans. A* **2004**, *35*, 1337.
- [157] K. Babinsky, R. De Kloe, H. Clemens, S. Primig, *Ultramicroscopy* **2014**, *144*, 9.
- [158] A. J. Breen, K. Babinsky, A. C. Day, K. Eder, C. J. Oakman, P. W. Trimby, S. Primig, J. M. Cairney, S. P. Ringer, *Microsc. Microanal.* **2017**, *23*, 279.
- [159] H. Xue, Y. Wu, F. Tang, X. Li, X. Lu, J. Ren, J. Li, *Mater. Today Commun.* **2022**, *31*, 103319.
- [160] H. Xue, Y. Luo, F. Tang, X. Lu, J. Ren, *Mater. Chem. Phys.* **2021**, *258*, 123977.
- [161] P. Zhou, J. Yu, X. Sun, H. Guan, Z. Hu, *Trans. Nonferrous Metals Soc. China* **2012**, *22*, 1594.
- [162] R. G. Menzies, R. H. Bricknell, A. J. Craven, *Philos. Mag. A* **1980**, *41*, 493.
- [163] N. G. Ingesten, R. Warren, L. Winberg, in *High Temperature Alloys for Gas Turbines 1982* (Eds: R. Brunetaud, D. Coutsouradis, T.B. Gibbons, Y. Lindblom, D.B. Meadowcroft, R. Stickler), Springer Netherlands, Dordrecht **1982**, p. 1013.
- [164] J. S. Crompton, R. W. Hertzberg, *J. Mater. Sci.* **1986**, *21*, 3445.
- [165] W. Ma, G. Liu, B. Hu, Y. Zhang, J. Liu, *Mater. Sci. Eng. A* **2013**, *587*, 313.
- [166] L. Tan, G. He, F. Liu, Y. Li, L. Jiang, *Materials* **2018**, *11*, 328.
- [167] Y. Li, H. Liu, J. Liu, Z. Wang, Y. Hao, *China Foundry* **2011**, *9*, 6.
- [168] P. Villars, K. Cenzual, SpringerMaterials **2012**, sd\_0261187.
- [169] Y. Murata, N. Yukawa, *Scr. Metall.* **1986**, *20*, 693.
- [170] P. Villars, K. Cenzual, SpringerMaterials **2012**, sd\_0304985.
- [171] P. Villars, K. Cenzual, SpringerMaterials **2012**, sd\_0261059.
- [172] R. C. Reed, M. P. Jackson, Y. S. Na, *Metall. Mater. Trans. A* **1999**, *30*, 521.
- [173] E. H. Van der Molen, J. M. Oblak, O. H. Kriege, *Metall. Mater. Trans. B* **1971**, *2*, 1627.
- [174] S. A. Croxall, M. C. Hardy, H. J. Stone, P. A. Midgley, in *Proc. of the 1st Int. Conf. on 3D Materials Science* (Eds: M. De Graef,

- H. F. Poulsen, A. Lewis, J. Simmons, G. Spanos), Springer International Publishing, Cham **2012**, pp. 215–220.
- [175] K. A. Green, J. A. Lemsky, R. M. Gasior, in *Superalloys 1996 (Eighth International Symposium)*, **1996**, p. 697.
- [176] S. E. Kim, M. P. Jackson, R. C. Reed, C. Small, A. James, N. K. Park, *Mater. Sci. Eng. A* **1998**, 245, 225.
- [177] H. Fecht, D. Furrer, *Adv. Eng. Mater.* **2000**, 2, 777.
- [178] S. K. Jain, B. A. Ewing, C. A. Yin, in *Superalloys 2000 (Ninth International Symp.)*, **2000**, p. 785.
- [179] H. Liu, N. Ta, M. Xu, Y. Meng, G. Xu, L. Zheng, *J. Mater. Eng. Perform.* **2020**, 29, 7940.
- [180] A. M. Volkov, M. M. Karashaev, M. N. Letnikov, M. M. Bakradze, *Russ. Metall.* **2019**, 2019, 1497.
- [181] J. Radavich, D. Furrer, T. Carneiro, J. Lemsky, in *Superalloys 2008 (Eleventh International Symposium)* **2008**, p. 63.
- [182] R. John, C. Tadeu, F. David, L. Joseph, B. Anthony, *Chinese J. Aeronaut.* **2007**, 20, 97.
- [183] S. Benhadad, N. L. Richards, M. C. Chaturvedi, *Metall. Mater. Trans. A* **2002**, 33, 2005.
- [184] T. Alam, P. J. Felber, M. Chaturvedi, L. T. Stephenson, M. R. Kilburn, J. M. Cairney, *Metall. Mater. Trans. A* **2012**, 43, 2183.
- [185] J. W. Gibbs, in *The Collected Works of J. Willard Gibbs*, Longmans, Green And Co., New York, London **1928**.
- [186] I. Langmuir, *J. Am. Chem. Soc.* **1918**, 40, 1361.
- [187] D. McLean, A. Maradudin, *Phys. Today* **1958**, 11, 35.
- [188] E. D. Hondros, M. P. Seah, *Int. Metals Rev.* **1977**, 22, 262.
- [189] J. W. Cahn, J. E. Hilliard, *Acta Metall.* **1959**, 7, 219.
- [190] M. Guttman, *Philos. Trans. Roy. Soc. Lond. Series A, Math. Phys. Sci.* **1980**, 295, 169.
- [191] M. Guttman, *Surf. Sci.* **1975**, 53, 213.
- [192] M. P. Seah, *Acta Metall.* **1977**, 25, 345.
- [193] J. Dong, M. Zhang, X. Xie, R. G. Thompson, *Mater. Sci. Eng. A* **2002**, 328, 8.
- [194] R. Ding, *Mater. Sci. Technol.* **2010**, 26, 36.
- [195] L. Wang, R. D. Kamachali, *J. Alloys Compd.* **2023**, 933, 167717.
- [196] F. L. Williams, D. Nason, *Surface Sci.* **1974**, 45, 377.
- [197] P. Wynblatt, R. C. Ku, *Surf. Sci.* **1977**, 65, 511.
- [198] A. R. Miedema, *Int. J. Mater. Res.* **1978**, 69, 455.
- [199] G. Bozzolo, J. Ferrante, J. R. Smith, *Phys. Rev. B* **1992**, 45, 493.
- [200] G. Bozzolo, B. Good, J. Ferrante, *Surf. Sci.* **1993**, 289, 169.
- [201] A. M. Rodríguez, G. Bozzolo, J. Ferrante, *Surf. Sci.* **1994**, 307–309, 625.
- [202] M. Militzer, J. Wieting, *Scr. Metall. Mater.* **1993**, 28, 1043.
- [203] M. Militzer, Yu. N. Ivashchenko, A. V. Krajnikov, P. Lejček, J. Wieting, S. A. Firstov, *Surf. Sci.* **1992**, 261, 267.
- [204] J. Nguejio, F. Szymtka, S. Hallais, A. Tanguy, S. Nardone, M. Godino Martinez, *Mater. Sci. Eng. A* **2019**, 764, 138214.
- [205] F. Zhang, L. E. Levine, A. J. Allen, M. R. Stoudt, G. Lindwall, E. A. Lass, M. E. Williams, Y. Idell, C. E. Campbell, *Acta Mater.* **2018**, 152, 200.
- [206] R. E. Howard, A. B. Lidiard, *Acta Metall.* **1965**, 13, 443.
- [207] R. E. Howard, A. B. Lidiard, *Philos. Mag.* **1965**, 11, 1179.
- [208] R. G. Faulkner, S.-H. Song, P. E. J. Flewitt, *Mater. Sci. Technol.* **1996**, 12, 904.
- [209] T. Shinoda, T. Nakamura, *Acta Metall.* **1981**, 29, 1631.
- [210] T. Shinoda, T. Nakamura, *Acta Metall.* **1981**, 29, 1637.
- [211] H. Rauh, R. Bullough, *Proc. R. Soc. Lond. A* **1985**, 397, 121.
- [212] R. Schafrik, R. Sprague, *KEM* **2008**, 380, 113.
- [213] Y. Wu, C. Li, X. Xia, H. Liang, Q. Qi, Y. Liu, *J. Mater. Sci. Technol.* **2021**, 67, 95.
- [214] O. M. Messé, J. S. Barnard, E. J. Pickering, P. A. Midgley, C. M. F. Rae, *Philos. Mag.* **2014**, 94, 1132.
- [215] J. Sharma, A. Nicolay, M. De Graef, N. Bozzolo, *Mater. Character.* **2021**, 176, 111105.
- [216] N. Saunders, M. Fahrman, C. J. Small, in *Superalloys 2000 (Ninth International Symposium)*, **2000**, p. 803.
- [217] S. Antonov, J. Huo, Q. Feng, D. Isheim, D. N. Seidman, R. C. Helmink, E. Sun, S. Tin, *Mater. Sci. Eng. A* **2017**, 687, 232.
- [218] J. Belan, *Mater. Today: Proc.* **2016**, 3, 936.
- [219] L. A. Gypen, A. Deruytere, *J. Mater. Sci.* **1977**, 12, 1028.
- [220] H. A. Roth, C. L. Davis, R. C. Thomson, *Metall. Mater. Trans. A* **1997**, 28, 1329.
- [221] B.-I. Kang, C.-H. Han, Y.-K. Shin, J.-I. Youn, Y.-J. Kim, *J. Mater. Eng. Perform.* **2019**, 28, 7025.
- [222] C. Joseph, C. Persson, M. Hörnqvist Colliander, *Mater. Sci. Eng. A* **2017**, 679, 520.
- [223] S. Xu, J. I. Dickson, A. K. Koul, *Metall. Mater. Trans. A* **1998**, 29, 2687.
- [224] A. Szczotok, K. Rodak, *IOP Conf. Ser.: Mater. Sci. Eng.* **2012**, 35, 012006.
- [225] L. Jiang, W.-Z. Zhang, Z.-F. Xu, H.-F. Huang, X.-X. Ye, B. Leng, L. Yan, Z.-J. Li, X.-T. Zhou, *Mater. Des.* **2016**, 112, 300.
- [226] S. M. Seo, I. S. Kim, J. H. Lee, C. Y. Jo, H. Miyahara, K. Ogi, *Metall. Mater. Trans. A* **2007**, 38, 883.
- [227] L. Liliensten, S. Antonov, D. Raabe, S. Tin, B. Gault, P. Kontis, *Microsc. Microanal.* **2019**, 25, 2538.
- [228] H. R. Zhang, O. A. Ojo, M. C. Chaturvedi, *Scr. Mater.* **2008**, 58, 167.
- [229] H. Zhang, Y. Wang, R.R. De Vecchis, W. Xiong, *J. Mater. Process. Technol.* **2022**, 305, 117597.
- [230] T. Wojcik, M. Rath, E. Kozeschnik, *Mater. Sci. Technol.* **2018**, 34, 1558.
- [231] W. Chen, M. C. Chaturvedi, N. L. Richards, G. McMahon, *Metall. Mater. Trans. A* **1998**, 29, 1947.
- [232] L. Xiao, D. Chen, M. C. Chaturvedi, *J. Mater. Eng. Perform.* **2005**, 14, 528.
- [233] E. Eriksson, M. Hörnqvist Colliander, *Metals* **2021**, 11, 122.
- [234] T. P. McAuliffe, I. Bantounas, L. R. Reynolds, A. Foden, M. C. Hardy, T. B. Britton, D. Dye, *Metall. Mater. Trans. A* **2021**.
- [235] A. Ramakrishnan, G. P. Dinda, *Mater. Sci. Eng. A* **2019**, 748, 347.
- [236] H. E. Collins, *Am. Soc. Metals* **1969**, 62.
- [237] K. A. Christofidou, H. T. Pang, W. Li, Y. Pardhi, C. N. Jones, N. G. Jones, H. J. Stone, in *Superalloys 2020* (Eds: S. Tin, M. Hardy, J. Clews, J. Cormier, Q. Feng, J. Marcin, C. O'Brien, A. Suzuki), Springer International Publishing, Cham **2020**, p. 1014.
- [238] A. S. Wilson, K. A. Christofidou, A. Evans, M. C. Hardy, H. J. Stone, *Metall. Mater. Trans. A* **2019**, 50, 5925.
- [239] K.-Y. Shin, J.-H. Kim, M. Terner, B.-O. Kong, H.-U. Hong, *Mater. Sci. Eng. A* **2019**, 751, 311.
- [240] D. Kim, R. Jiang, A. Evangelou, I. Sinclair, P. A. S. Reed, *Int. J. Fatigue* **2021**, 145, 106086.
- [241] K. L. More, M. K. Miller, *J. Phys. Colloques* **1988**, 49, C6.
- [242] Y. S. Na, N. K. Park, R. C. Reed, *Scr. Mater.* **2000**, 43, 585.
- [243] L. Chang, H. Jin, W. Sun, *J. Alloys Compd.* **2015**, 653, 266.
- [244] Y. S. Zhao, J. Zhang, Y. S. Luo, J. Li, D. Z. Tang, *Mater. Sci. Eng. A* **2016**, 672, 143.
- [245] R. Jiang, Y. D. Song, P. A. Reed, *Int. J. Fatigue* **2020**, 141, 105887.
- [246] A. Pineau, S. D. Antolovich, *Eng. Failure Anal.* **2009**, 16, 2668.
- [247] N. L. Richards, M. C. Chaturvedi, *Int. Mater. Rev.* **2000**, 45, 109.
- [248] E. Chauvet, P. Kontis, E. A. Jäggle, B. Gault, D. Raabe, C. Tassin, J.-J. Blandin, R. Dendievel, B. Vayre, S. Abed, G. Martin, *Acta Mater.* **2018**, 142, 82.
- [249] R. Kataria, R. Pratap Singh, P. Sharma, R. K. Phanden, *Mater. Today: Proc.* **2021**, 38, 265.
- [250] M. Kolb, L. P. Freund, F. Fischer, I. Povstugar, S. K. Makineni, B. Gault, D. Raabe, J. Müller, E. Spiecker, S. Neumeier, M. Göken, *Acta Mater.* **2018**, 145, 247.

- [251] I. Taji, T. Hajilou, A. S. Ebner, D. Scheiber, S. Karimi, E. Plesiutchnig, W. Ecker, A. Barnoush, V. Maier-Kiener, R. Johnsen, V. I. Razumovskiy, *Corros. Sci.* **2022**, *203*, 110331.
- [252] W. D. Summers, E. Alabort, P. Kontis, F. Hofmann, R. C. Reed, *Mater. High Temp.* **2016**, *33*, 338.
- [253] G. A. Zickler, R. Radis, R. Schnitzer, E. Kozeschnik, M. Stockinger, H. Leitner, *Adv. Eng. Mater.* **2010**, *12*, 176.
- [254] W. V. Youdelis, O. Kwon, *Metal Sci.* **1983**, *17*, 385.
- [255] S. Vernier, A. Pugliara, B. Viguier, E. Andrieu, L. Laffont, *Metall. Mater. Trans. A* **2020**, *51*, 6607.
- [256] M. J. Kaufman, V. I. Levit, *Philos. Mag. Lett.* **2008**, *88*, 259.
- [257] V. V. Rielli, F. Theska, Y. Yao, J. P. Best, S. Primig, *Mater. Res. Lett.* **2022**, *10*, 301.
- [258] X. Song, Y. Wang, X. Zhao, J. Zhang, Y. Li, Y. Wang, Z. Chen, *J. Alloys Compd.* **2022**, *911*, 164959.
- [259] M. Göken, M. Kempf, *Acta Mater.* **1999**, *47*, 1043.
- [260] C. Ye, J. Chen, M. Xu, X. Wei, H. Lu, *Mater. Sci. Eng. A* **2016**, *662*, 385.
- [261] E. Alabort, D. Barba, S. Sulzer, M. Lišner, N. Petrinic, R. C. Reed, *Acta Mater.* **2018**, *151*, 377.
- [262] K. L. Auth, J. Brouzoulis, M. Ekh, *J. Mech. Phys. Solids* **2022**, *164*, 104880.
- [263] R. Brommesson, M. Ekh, C. Joseph, *Eng. Fract. Mech.* **2016**, *154*, 57.
- [264] V. V. Rielli, F. Theska, S. Primig, *Microsc. Microanal.* **2021**, *1*.
- [265] Y. Wei, Z. Peng, M. Kühbach, A. Breen, M. Legros, M. Larranaga, F. Momprou, B. Gault, *PLoS ONE* **2019**, *14*, 0225041.
- [266] D. J. Larson, T. J. Prosa, R. M. Ulfig, B. P. Geiser, T. F. Kelly, in *Local Electrode Atom Probe Tomography*, Springer New York, New York, NY **2013**.
- [267] K. Babinsky, W. Knabl, A. Lorich, R. De Kloe, H. Clemens, S. Primig, *Ultramicroscopy* **2015**, *159*, 445.
- [268] P. Felfer, V. Dalbauer, M. Heller, B. Ott, **2021**.



**Felix Theska** joined UNSW Sydney in 2016 after completing a master's in materials science at the University of Technology Ilmenau (Germany). He was awarded his Ph.D. on high-resolution characterization of strengthening effects in superalloys in 2020. Felix' key strengths are in industry-focused research on aerospace materials. He is an expert in high-resolution characterization methods including atom probe, TEM, and EBSD.



**Sophie** is currently a Scientia Associate Professor at UNSW Sydney. Her research contributions are in processing–structure–property relationships of structural alloys. She was awarded her Ph.D. from Montanuniversität Leoben (Austria) in 2012. After a short period of postdoctoral research and a role as leader of a group with strong industry linkages at the same university, she moved to UNSW in 2015. She holds two UNSW Grad Certs in Education and Management. She is a passionate student-focused teacher, editor of *Journal of Materials Science*, current TMS Phase Transformation Committee Vice Chair, and active Materials Australia member.